

Investigation of the Impact of Physical
Constraints Imposed by Flight Control
Actuation Systems on Aircraft
Multidisciplinary Design Optimization

Yuxiao Liu



Department of Mechanical Engineering
McGill University
Montréal, Québec, Canada

August 2023

A thesis presented for the degree of Masters of Science

©2023 Yuxiao Liu

Abstract

Flight control actuation systems (FCASs) have a considerable impact on aircraft design as they alter the geometrical definition of the wings and the tail. It is therefore necessary to integrate them into the aircraft multidisciplinary design optimization (MDO) process. In this work, an FCASs space envelope prediction tool was developed and integrated in an industrial MDO environment at the conceptual design phase. The tool uses control surfaces physical properties, including aerodynamic hinge moment and horn radius, with the addition of a knowledge-based statistical method constructed using embedded aircraft data to size primary and secondary FCASs. A business jet test case was considered. The aircraft is optimized with and without FCASs space envelope constraints to demonstrate the impact on optimal aircraft design. MDO results were obtained for different values of the FCASs space envelope constraints to perform sensitivity analysis of the MDO objective. An additional investigation was conducted to assess the potential of generating MDO results using Machine Learning models with validation sets given by previous experimental results.

Abrégé

Les systèmes d'actionnement des commandes de vol (FCAS) ont un impact considérable sur la conception des aéronefs car ils modifient la définition géométrique des ailes et de la queue. Dans ce travail, un outil de prédiction d'enveloppe spatiale FCAS a été développé et intégré dans un environnement MDO industriel lors de la phase de conception. L'outil utilise les propriétés physiques des surfaces de contrôle, y compris le moment de charnière aérodynamique et le rayon du cornet, avec l'ajout d'une méthode statistique basée sur la connaissance construite à l'aide de données d'avion embarquées pour dimensionner les FCAS primaires et secondaires. Un cas d'essai d'avion d'affaires a été envisagé. L'avion est optimisé avec et sans contraintes d'enveloppe spatiale FCAS pour démontrer l'impact sur la conception optimale de l'avion. Les résultats MDO ont été obtenus pour différentes valeurs des contraintes d'enveloppe spatiale FCAS afin d'effectuer une analyse de sensibilité de l'objectif MDO. Une enquête supplémentaire a été menée pour évaluer le potentiel de génération de résultats MDO à l'aide de modèles d'apprentissage automatique avec des ensembles de validation donnés par des résultats expérimentaux antérieurs.

Acknowledgements

First and foremost, I would like to express my sincere gratitude to my supervisor, Professor Michael Kokkolaras, for his continuous support and guidance during my studies at McGill University. He always found time to answer my questions and share his knowledge and resources.

I am grateful to Bombardier's Advanced Product Development department for supporting and sponsoring the work. Special acknowledgment is given to Ali Tfaily, who had been acting as my industrial supervisor and provided his insights on aircraft design and optimization. I would also like to thank Jasveer Singh, who shared his knowledge on Bombardier's conceptual multidisciplinary design optimization platform.

Finally, I am grateful to my family and friends for their unconditional love and confidence during my studies, and my whole life.

Contents

1	Introduction	1
1.1	Background and Motivation	1
1.2	Research Objectives	3
1.3	Thesis Organization	4
2	Literature Review	5
2.1	Aircraft MDO Considering Existing and New Disciplines	5
2.2	Modelling of Flight Control Actuation System	8
3	FCASs Space Envelope Prediction Models	11
3.1	System Envelope Sizing Method for Flaps	12
3.1.1	Fowler Type Flap System	13
3.1.2	Dropped Hinge Type Flap System	17
3.2	System Envelope Sizing Method for Slats	19
3.3	System Envelope Sizing Method for Spoilers	23

3.4	System Envelope Sizing Method for Primary Flight Controls	28
3.5	Model Validation and Uncertainty Quantification	35
4	Aircraft CMDO Workflow Overview	39
4.1	Aircraft CMDO Environment and Architecture	39
4.2	Aircraft CMDO Optimizer	43
4.3	Integrated FCASs Space Envelope Prediction Model within CMDO	46
5	Numerical Investigation and Results	49
5.1	Comparison of Obtained Designs	49
5.2	Optimal Design Sensitivity Analysis	55
5.3	Machine Learning-Based Sensitivity Analysis	58
6	Summary and recommendations	61

List of Figures

1.1	Example of perspective depending on their area of responsibility, adapted from [1]	2
1.2	Demonstration of relatively low cost incurred during conceptual design, adapted from [2]	3
3.1	Components of Fowler type flap system, adapted from [3]	13
3.2	Example of correlation analysis for carriage length sizing based on different types/configurations of aircraft	14
3.3	Illustration of fowler type flap track envelope length and height, adapted from [3]	15
3.4	High-level diagram of Fowler type flap system sizing method	16
3.5	Components of dropped hinge type flap system, adapted from [3]	17
3.6	High-level diagram of dropped hinge type flap system sizing method	19
3.7	Slat system schematic and space envelope parameters of interests, adapted from [4]	20

3.8	Definition of slat chord, WUSS chord, and hinge radius, adapted from [4] . . .	21
3.9	High-level diagram of slat system sizing method	23
3.10	Different types of spoiler actuator mountings	24
3.11	Example of space envelope definition for a common spoiler actuator	25
3.12	System installation schematic for horn radius estimation	26
3.13	High-level diagram of spoiler system sizing method	28
3.14	Example of linear and rotary vane actuators for primary flight controls [5] . .	29
3.15	PFC system schematic and space envelope parameters of interests	30
3.16	High level diagram of primary flight control system sizing method	34
3.17	Example of determining correction factor value for PFC hinge moment estimation	36
3.18	Random variable modelling for Aileron actuation system space envelope estimation	38
3.19	Monte-Carlo simulation of aileron PCU envelope height distribution	38
4.1	Schematic of aircraft MDO problem with integration of FCASs sizing discipline	41
4.2	Sequence of discipline evaluation within current MDO formulation with chosen sequence addition of FCASs Sizing	42
4.3	Overview of the general surrogate-based optimization algorithm, adapted from [6]	43

4.4	Illustration of one step DoE enrichment and surrogate model adaptation on an example of one-dimensional Forrester function. (a) Kriging prediction and the location of the next update DoE, (b) Infill criterion (Expected Improvement, EI), adapted from [7]	45
4.5	Schematic showing data-flow of FCASs sizing module within CMDO environment and post-processing	48
5.1	Optimal wing and tail planform designs with and without FCASs constraints	51
5.2	Optimal wing airfoil designs with and without FCASs constraints at (a) 57% spanwise location and (b) 89% spanwise location.	52
5.3	Location of flight control surfaces and corresponding FCASs of the optimal aircraft design with FCASs constraints	55
5.4	Sensitivity analysis results	56
5.5	Training and prediction generation process for SEGOMOE ML model	59
5.6	ML-based results for MTOW sensitivity to selected FCASs space envelope constraints	60

List of Tables

5.1	Variance of optimization results obtained with FCASs constraints comparing to the results obtained without FCASs constraints	50
5.2	Comparison of optimization results with and without FCASs constraints . .	54
5.3	Constraints to be investigated and their corresponding reference value	56
5.4	Sensitivity analysis results	58
5.5	MTOW sensitivity results comparison	60

Nomenclature

Acronyms

CBO Constrained Bayesian Optimization

CDF Cumulative Distribution Function

CFD Computational Fluid Dynamics

CMDO Conceptual Multidisciplinary Design Optimization

CoG Center of Gravity

DoE Design of Experiments

EHSA Electro-Hydrostatic Actuator

EI Expected Improvement infill criterion

EMA Electro-Mechanical Actuator

FCASs Flight Control Actuation Systems

FEM Finite Element Method

GS Ground Spoilers

HMA Hydro-Mechanical Actuators

LVDT Linear Variable Differential Transformer

MDO Multidisciplinary Design Optimization

MFS Multi-Function Spoilers

ML Machine Learning

MOE Mixture of Experts

MTOW Maximum Take-off Weight

OML Outer Mold Line

ONERA French Aerospace Research Lab

PCU Primary Control Unit

PFC Primary Flight Control

SEGOMOE Super Efficient Global Optimization with Mixture of Experts

WUSS Wing Under Slat Surface

Symbols

α angle of attack

δ control surface deflection

δ_{\max} maximum control surface deflection

ρ air density

σ_{req} required stress on PCU rod

A_{cs} control surface area

A_{piston} PFC actuator piston area

C_{cs} control surface mean chord length

$c_{\text{h}\alpha}$ hinge moment coefficient related to angle of attack

$c_{\text{h}\delta}$ hinge moment coefficient related to control surface deflection

C_{WUSS} wing under slat surface mean chord

d_{actS} slat actuator envelope diameter

d_{rod} PFC piston rod diameter

F_{aero} aerodynamic load

H_{actSP} spoiler actuator envelope height

H_{PCU} PFC PCU envelope height

H_{trackF} fowler type flap track envelope height

H_{trackS} slat track envelope height

ID_{PFC} PFC piston cylinder inner diameter

ID_{SP} spoiler actuator cylinder inner diameter

L_{actSP} spoiler actuator envelope length

$L_{\text{carriageF}}$ fowler type flap carriage envelope length

L_{PCU} PFC PCU envelope length

L_{trackF} fowler type flap track envelope length

L_{trackS} slat track envelope length

M_{H} hinge moment

M_{OM} maximum operating mach number

OD_{PFC} PFC piston cylinder outer diameter

OD_{SP} spoiler actuator cylinder outer diameter

r_{hinge} hinge radius

r_{horn} horn radius

T_{trackS} slat track thickness

v aircraft speed

V_{fe} maximum aircraft velocity with flaps fully extended

V_{ref} aircraft reference approach speed

Chapter 1

Introduction

1.1 Background and Motivation

Modern aircraft conceptual design involves simultaneous consideration of multiple interacting disciplines. Variables are often shared by more than one discipline and outputs of one discipline often flow into another as inputs. This feedback loop leads to the formulation of multidisciplinary design optimization (MDO) problems. Typical disciplines considered in an aircraft conceptual MDO (CMDO) problem include aerodynamics, weights and balance, production cost, stability and control, propulsion, and more. Aircraft CMDO allows designers to maintain a comprehensive perspective of the aircraft design during the conceptual phase to avoid the view being dominated by one discipline only (Figure 1.1).

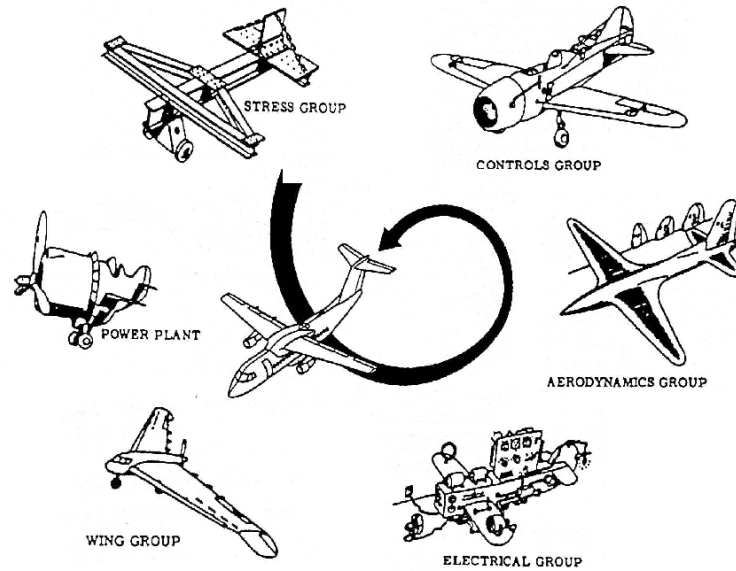


Figure 1.1: Example of perspective depending on their area of responsibility, adapted from [1]

The significance of aircraft conceptual design, in comparison with later product development phases, lies in the ease of change in design and relatively low cost in doing so (Figure 1.2). It is therefore important to increase the maturity of the product during conceptual design in order to mitigate the risk of re-design in later phases, which incurs higher level of cost and consumption of human resources. In the context of CMDO, one of the approaches in pursuit of such goal is to include additional disciplinary considerations and constraints to generate more conservative optimal design.

Fight control actuation systems (FCASs) become candidates to be included in aircraft CMDO due to the significant impact of FCASs installation on aircraft wing and tail design and aircraft weight. The FCASs studied in this work include flap systems, slat systems,

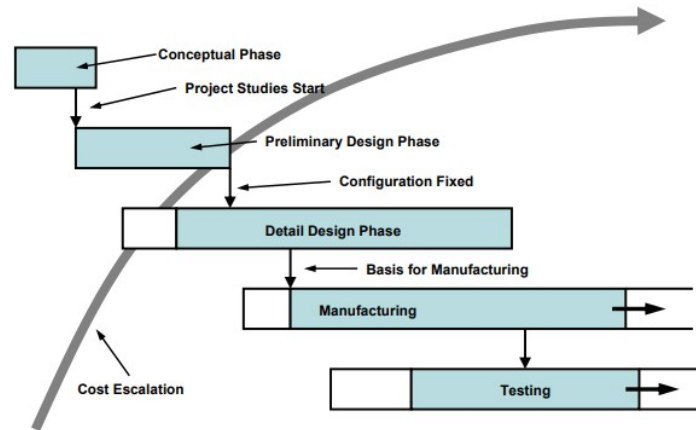


Figure 1.2: Demonstration of relatively low cost incurred during conceptual design, adapted from [2]

spoiler systems, and primary flight control (PFC) systems. This research focuses on the space envelope occupied by FCASs and the related system integration constraints required to be added to the existing CMDO environment. The existing CMDO environment is built using the Dassault Systemes Isight [8] software and already includes several disciplinary models.

1.2 Research Objectives

The objectives of this research are listed as below:

- Develop and automate a set of FCASs space envelope sizing methods that take aircraft- and system-level inputs within CMDO environment.
- Integrate FCASs installation physical constraints into existing CMDO environment

and achieve more mature product definition in early design stage.

- Assess the sensitivity of aircraft CMDO objective function to the changes in FCASs installation physical constraints.

1.3 Thesis Organization

The thesis is organized as follows. Chapter 2 presents a literature review on aircraft MDO research development with focus on disciplines that had been considered and the modelling methodology for modern flight control actuators and actuation systems. Chapter 3 details the FCASs modelling approach developed in this work, with purpose of space envelope sizing. The CMDO environment is introduced in Chapter 4, including the existing disciplinary models, the optimization algorithm, and the additional constraints introduced by the integration of FCASs sizing module in the CMDO framework. Chapter 5 presents the setup and results of numerical experiments to discuss the impact of FCASs integration on aircraft design and weight. The thesis concludes with a summary on achievements and limitations as well as suggestions for future work in Chapter 6.

Chapter 2

Literature Review

2.1 Aircraft MDO Considering Existing and New Disciplines

In early initiatives, the main objective of aircraft multi-disciplinary design optimization was to develop more efficient wing planform designs via the coupling of high-fidelity, multi-physics models focusing mainly on aerostructural domain [9–13]. While the capabilities of high-fidelity aerostructural optimization continue to improve [14–17], aircraft MDO has now reached widespread application in industrial environments, including the conceptual, preliminary, detailed design phases [18]. The deployment of a multi-level MDO framework in line with the aircraft design stages in an industrial environment is presented in [19]. It introduces disciplinary models used in a typical CMDO problem: a quasi-3D aerodynamics

model, knowledge-based weight prediction, and fixed-architecture scaled engine model. Tools of relatively higher fidelity are also used in aircraft CMDO work, including surrogate models built using data generated from high-fidelity simulations [20, 21]. In general, the objective and deliverable of aircraft CMDO is to explore design space and establish a baseline reference configuration in a time efficient manner, and therefore simulation fidelity is traded for number of disciplines and design variables included considering limited computational budgets.

The most commonly seen disciplines in an aircraft MDO problem include aerodynamics, the estimation of weight and structural response, and propulsion. Empirical (knowledge) and panel methods-based predictions are typically used as low-fidelity aerodynamic models [22–24], while some frameworks use computational fluid dynamics (CFD)-based aerodynamic models [16, 25, 26]. Similarly, weight and balance estimation within an MDO environment can be conducted through low-fidelity analysis [22, 23, 27] or high-fidelity models augmented by structural analysis [28]. The analysis of structures is typically only included in detailed design stages where increased fidelity is required [19]; therefore, the structural models seen in an aircraft MDO work are usually based on global or detailed finite element analysis (FEA) [25, 26, 28–30]. To this date, the finite-element based structural analyses are solely focused on the wing [30], and their main advantage within a MDO framework is that they can be used either to directly calculate the structural strength [30] or to provide additional data for further static as well as dynamic aeroelastic computations [31]. Finally, propulsion models can be built using statistical and empirical approximations [32] or supplier data [19]. The

“rubberized” engines as low fidelity models can also be built using engine scaling factors [33]. For higher fidelity level optimizations, a real engine model built with full or partial engine simulation is typically used [34–36]. Apart from above mentioned disciplines, there exists a set of supplementary models that are identified as common. They are typically used as support elements to enhance and complement the calculations within the optimization loop. One example of this that can be seen in most MDO frameworks is a stability and control (trim) model. A simple way to achieve trimmed state is through iterations of control surfaces parameters [23,37], and stability can be empirically evaluated on the basis of stability derivatives [38] or static margin [27,39]. Secondly, with weight, propulsion and aerodynamic becoming available, a mission performance discipline can be evaluated. With a specified set of steps to accomplish mission, the required energy to fly each segment is calculated analytically [27,40,41] or through numerical simulations [22,42].

The scope of aircraft MDO has also expanded over time to include an alternative set of disciplines. The environmental performance discipline has drawn interest in recent developments. An aerial vehicle impacts the environment in two ways: Emission of harmful gases through fuel burn [27,35,36,43,44] and generation of noise by engine and airframe while on ground [25,44–46], especially for the design cases of supersonic jets [28,43,47–49]. The common quantification approach for noise propagation is through analytical calculation [43], while for emission calculation is through empirical equations [27,43] and advanced finite element methods [28,47,48]. One advantage of environmental performance

consideration is to help engineers determine if a given design satisfies airport and community regulations regarding noise and emission. Another discipline that is seldom considered in MDO is aircraft subsystem simulations, which typically includes hydraulics [50], environmental control [33, 51, 52], and fuel supply [52]. Consideration of such discipline not only introduces necessary additional system weight to be included, but also models the interaction between systems. For example, the degradation of engine performance due to air bleeding requirements of environmental control system [33]. Further beneficial additions includes economics discipline to estimate the R&D, production, and operation costs [27, 35, 53, 54] and bridge the gap between technical and financial disciplines, landing gear integration module to consider related physical constraints [55, 56], and electromagnetics to quantify the airframe radar signature for military projects' purposes [57, 58].

2.2 Modelling of Flight Control Actuation System

Over the decades, the industry has been trending towards more electric aircraft design with fly-by-wire flight control configuration. While some research topics remains open, including design of hybrid gas-electric propulsion aircraft [59], electric taxi capability without the use of tug vehicle [60], application of fuel cell in replacement of turbines [61], and improvement of electric power distribution performance to decrease necessary system redundancies [62], the modelling and sizing of more-electric FCASs has gained certain level

of maturity. Diaz et al. developed a sizing workflow for electro-hydrostatic actuators (EHSAs) and electro-mechanical actuators (EMAs), both commonly-seen in fly-by-wire architecture [63, 64]. The sizing is performed through a mixture of physics-based and knowledge-based methods, using the aerodynamic force that the (equivalent) actuator cylinder is subject to as main input. The work then extends to the development of CATIA-based parametric models for EHSAs and EMAs using output from the sizing model to perform rapid 3D modelling. Using a similar approach, more functionalities can be added to an actuator envelope sizing model. Weight prediction for EHSAs can also be done using statistical-based estimation [65–67]; power consumption prediction is conducted with additional flight condition input [52].

From a systems engineering (SE) perspective, the modelling of electric FCASs has been considered in the literature. Fu et al. developed SE approaches for EMA based FCAS model architecting and multi-purpose incremental modelling [68]. An aileron actuation system case study is used to illustrate the approach, including energy consumption, thermal analysis, and fault response. Di Rito et al. developed object-oriented modelling and sizing approaches in Modelica-Dymola environment for both more electric FCASs and conventional hydro-mechanical FCASs [69]. Performance comparison is then performed and the superiority of the EMA based FCAS is demonstrated in terms of energy savings.

This thesis contributes to the above mentioned SE domain by developing a comprehensive sizing framework for all primary and secondary FCASs with an electric or a hydro-mechanical

architecture. Moreover, a study that integrates physical flight control actuation system constraints into aircraft MDO at the conceptual design stage has not been conducted yet to the best of our knowledge.

Chapter 3

FCASs Space Envelope Prediction

Models

Modelling efforts for this work aimed at developing physics- and knowledge-based models to estimate FCASs system envelope during the conceptual design phase. Depending on the flight control system of interest, the FCASs system envelope can include primary control unit (PCU), actuator box, track, carriage, and/or hinge arm. In this section, the architecture of modelling and space envelope estimation approach for each considered flight control system is described. The models are built using C++ and integrated into the Isight framework of the existing MDO environment as an executable file. The work is built on the basis of existing knowledge-based sizing methods for spoilers.

For all flight control systems, the approach starts with the calculation of aerodynamic

hinge moment (M_H), or aerodynamic load

$$M_H = A_{cs} \cdot C_{cs} \cdot \frac{\rho}{2} v^2 \cdot (c_{h\alpha} \cdot \alpha + c_{h\delta} \cdot \delta), \quad (3.1)$$

where A_{cs} and C_{cs} are area and average chord of control surface, ρ is air density, v is aircraft speed, $c_{h\alpha}$ is hinge moment coefficient related to angle of attack, $c_{h\delta}$ is hinge moment coefficient related to control surface deflection, α is angle of attack and δ is control surface deflection [4]. The aerodynamic load on FCASs is assumed to be highly correlated with FCASs dimensions, neglecting control surface inertia since it is relatively small. During the early design phase, It is desired to reduce the number of flight conditions dependent variables as they are not available without performing real-time flight dynamics analysis in later development phase; therefore, estimation equations for aerodynamic load are sought to eliminate the presence of dynamic pressure ($\frac{\rho}{2}v^2$) and hinge moment coefficient ($c_{h\alpha} \cdot \alpha + c_{h\delta} \cdot \delta$). The reformulation of Equation 3.1 for each different flight control system will be introduced in the following sections.

3.1 System Envelope Sizing Method for Flaps

Space envelope estimation for flaps actuation system was separated between different flap deployment mechanisms. Two commonly seen mechanisms are considered in this work: Fowler types and dropped hinge types.

3.1.1 Fowler Type Flap System

Fowler type works by extending flaps out on rails or tracks. The system is composed of carriages, tracks, and actuators, as shown in Figure 3.1.

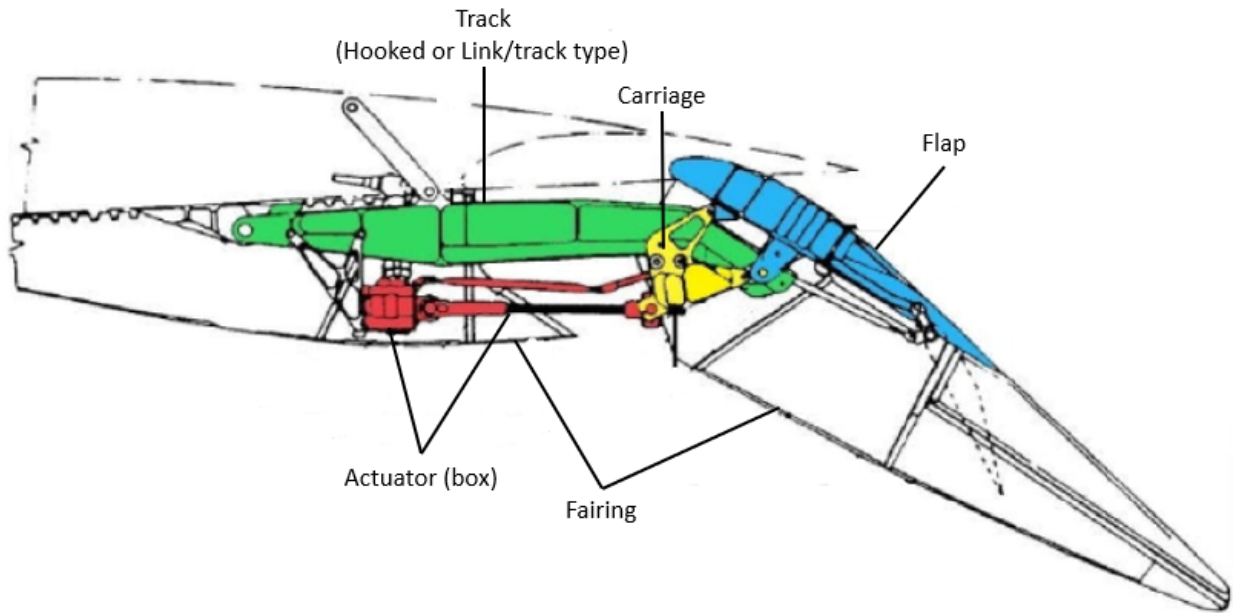


Figure 3.1: Components of Fowler type flap system, adapted from [3]

In order to size the actuator box and carriages, an estimated hinge moment is required as mentioned in Section 3. For flap systems, the equation becomes

$$M_H = A_{cs} \cdot C_{cs} \cdot V_{fe}^2 \cdot \delta_{max}, \quad (3.2)$$

where V_{fe} is the maximum aircraft velocity with flaps fully extended, and δ_{max} is the corresponding flap deflection. All required inputs in Equation 3.2 can be supplied by 1) aerodynamic and wing design analysis, which also determines position of flap panels, 2) performance, stability and control analysis, and 3) fixed design choice, including number of

flap panels.

The space envelope of carriages and actuation box is assumed to be directly correlated with aerodynamic hinge moment. As shown in Fig. 3.2, the data are known from existing aircraft, and prediction can be done using the correlation a linear model.

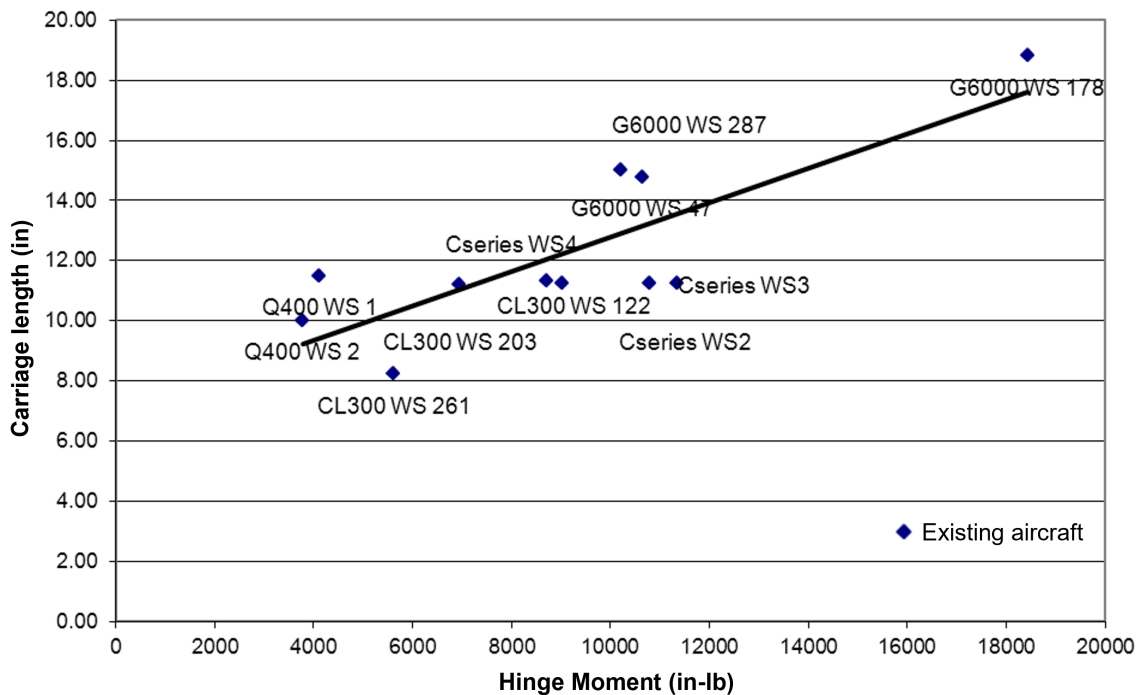


Figure 3.2: Example of correlation analysis for carriage length sizing based on different types/configurations of aircraft

Track space envelope for Fowler type flaps can be more accurately estimated by looking at geometry and kinematics of deployment. Flap track is attached to the rear spar, and extends depending on the distance travelled by the flap from zero to full deployment. The

flap track length and height envelope considering track deployment motion is shown in Fig.

3.3.

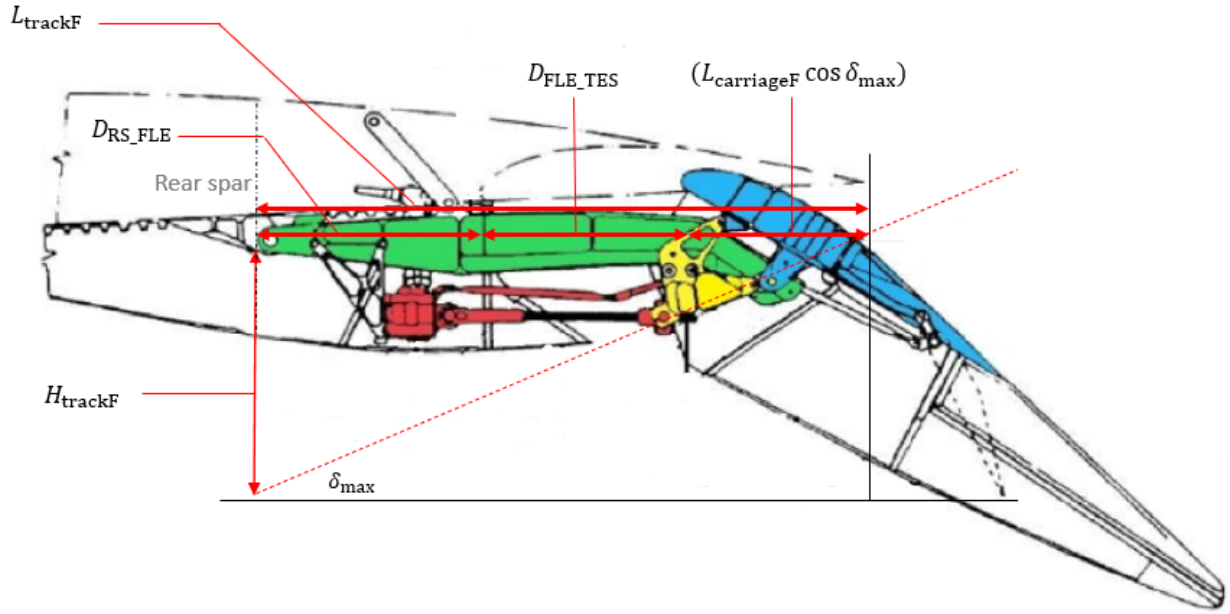


Figure 3.3: Illustration of fowler type flap track envelope length and height, adapted from [3]

In Figure 3.3, D_{RS_FLE} is the distance between rear spar and flap leading edge at retracted position, D_{FLE_TES} is the distance between flap leading edge and wing trailing edge shroud. The flap track envelope length and height are then

$$L_{trackF} = D_{RS_FLE} + D_{FLE_TES} + L_{carriageF} \cos \delta_{max} \quad (3.3)$$

and

$$H_{trackF} = L_{trackF} \tan \delta_{max}. \quad (3.4)$$

The track envelope width is estimated using correlation with aerodynamic hinge moment

as in Fig. 3.2. Another output of interest for flap systems is the flap track fairing wetted area. Intuitively, this can be correlated with enclosed area of track space envelope, which is calculated using track space envelope length, width and height. To summarize, the sizing flowchart for Fowler types flap system is shown in Fig. 3.4.

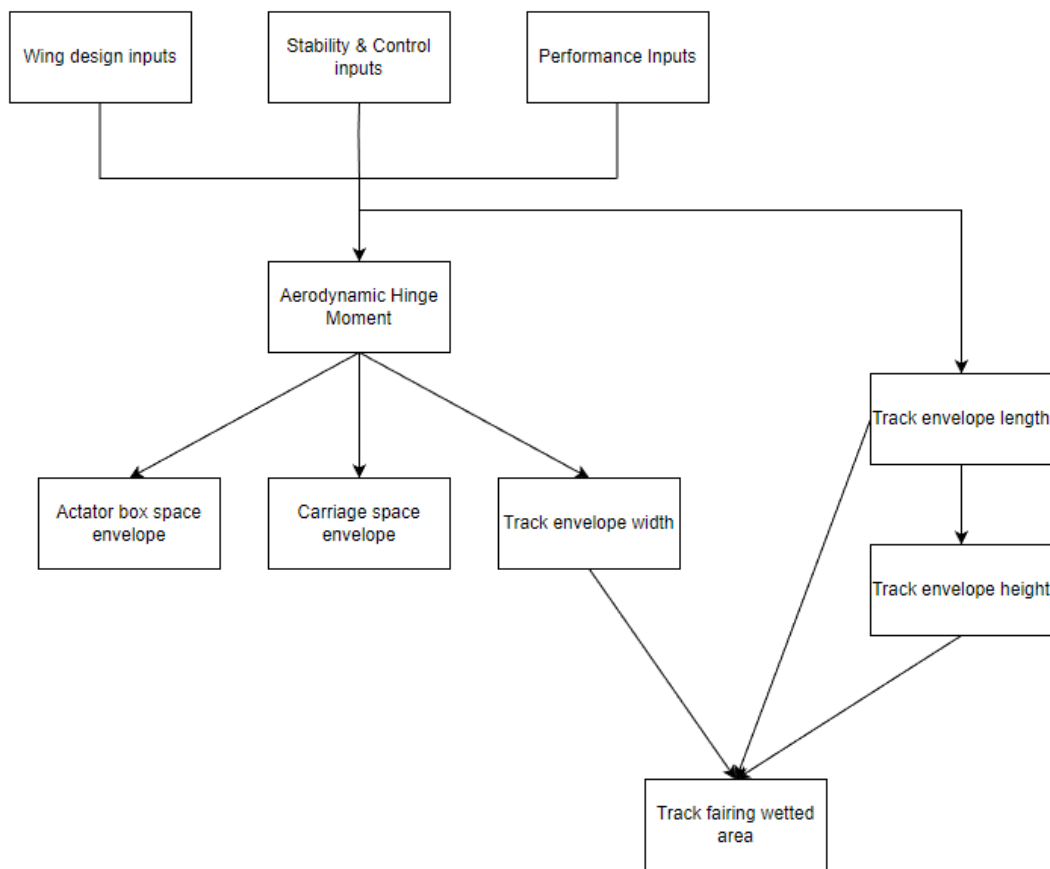


Figure 3.4: High-level diagram of Fowler type flap system sizing method

3.1.2 Dropped Hinge Type Flap System

The dropped hinge flap is characterized by a simple mechanism of a flap connected to a fixed hinge and pure rotational movement. Flap supports for this type consist of a hinge arm that is attached to the rear spar, a support link between the arm and the flap, and a hydraulic actuator. Fig. 3.5 shows the sketch and components of a typical dropped hinge type flap system.

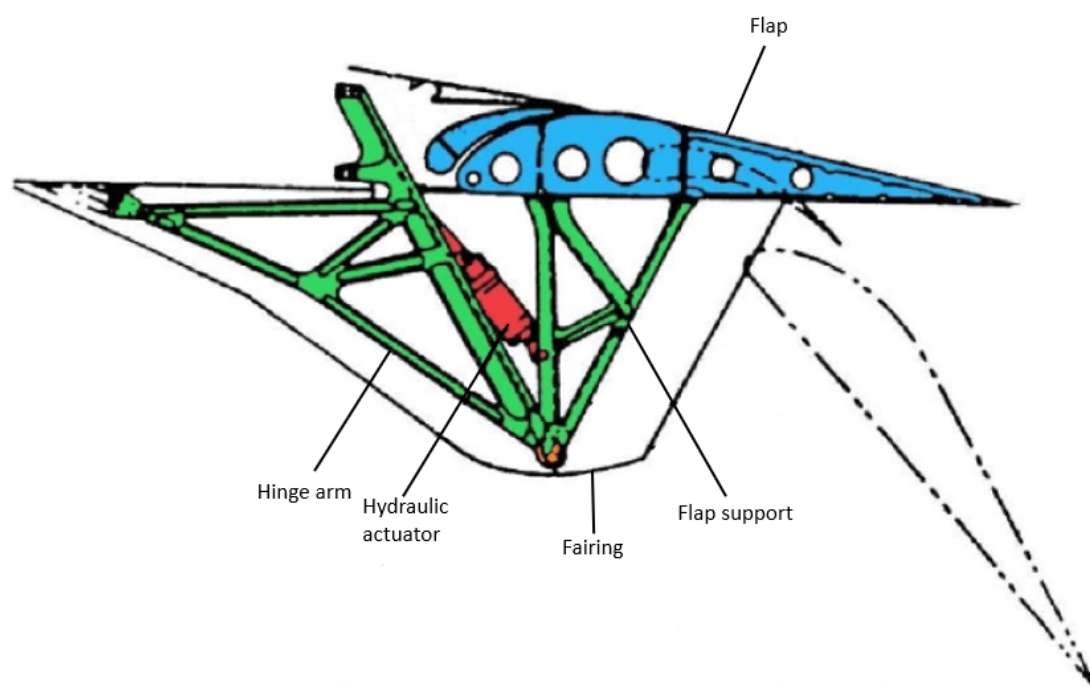


Figure 3.5: Components of dropped hinge type flap system, adapted from [3]

Since the hinge arm is the only mechanism connected to rear spar (and therefore interacting with wing design and the general aircraft design process), only the space envelope of the hinge arm is considered in the sizing process.

The aerodynamic hinge moment calculation is similar to that for Fowler type flaps as Equation 3.2, and hinge arm envelope height can be predicted by determining its correlation with hinge moment. Since the hinge arm is fixed and incapable of performing any motion (rotary motion is done by flap support for deployment), its envelope length is simply the distance between the leading edge of a retracted flap and the rear spar. For the width envelope, a correlation with flap panel area is sought due to the lower R^2 value found comparing to that with hinge moment. The dropped hinge flap fairing wetted area can then be predicted with obtained hinge arm space envelope enclosed area, similarly to the procedure outlined in Section 3.1.1.

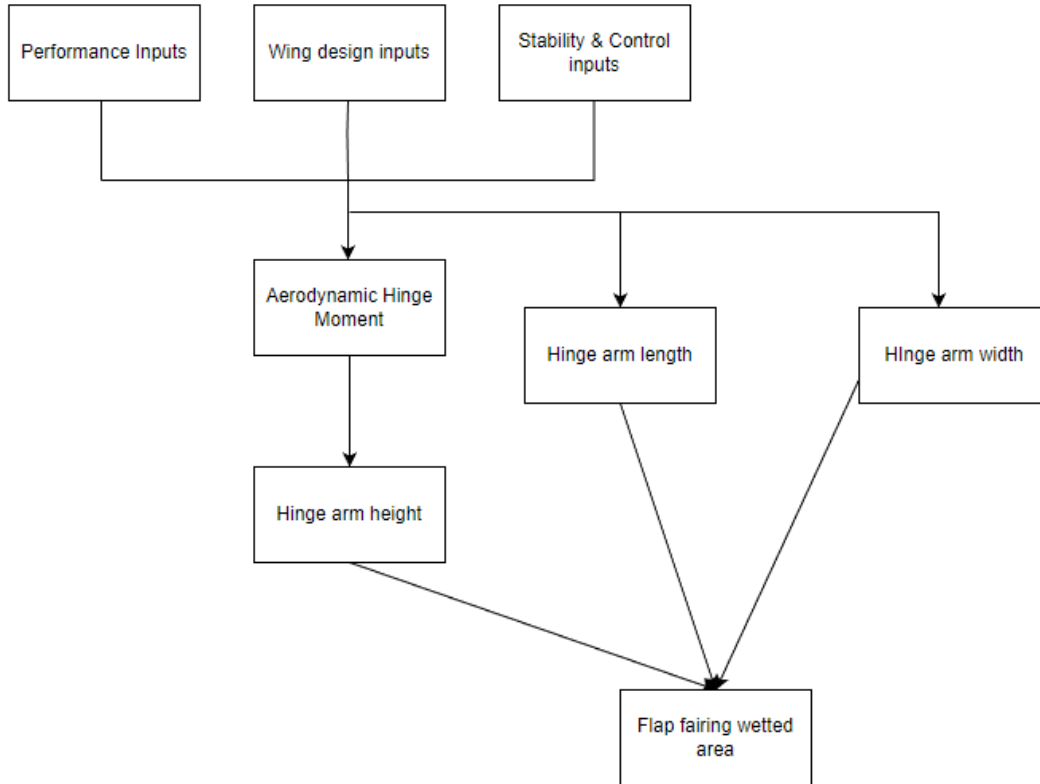


Figure 3.6: High-level diagram of dropped hinge type flap system sizing method

3.2 System Envelope Sizing Method for Slats

Based on the differences in deployment mechanism, slat actuation systems can be separated into linear type and rotary type. In this work, only rotary type actuators (or two-position actuator) are considered since this is the type that will be widely used on modern and future aircraft [4]. The rotary type actuator works by transferring the rotary motion of drive shaft to an attached track that is connected to the slat panel in order to control the position of

slats. A schematic of the slat system is shown in Fig. 3.7. Space envelope parameters of interests are identified considering wing thickness constraints on slat system integration: The first constraint is the actuator envelope diameter (d_{actS}) in addition to the track thickness (T_{trackS}) should be enclosed by height of front spar, and the second constraint is the retracted track space envelope (L_{trackS} and H_{trackS}) should be enclosed by the airfoil.

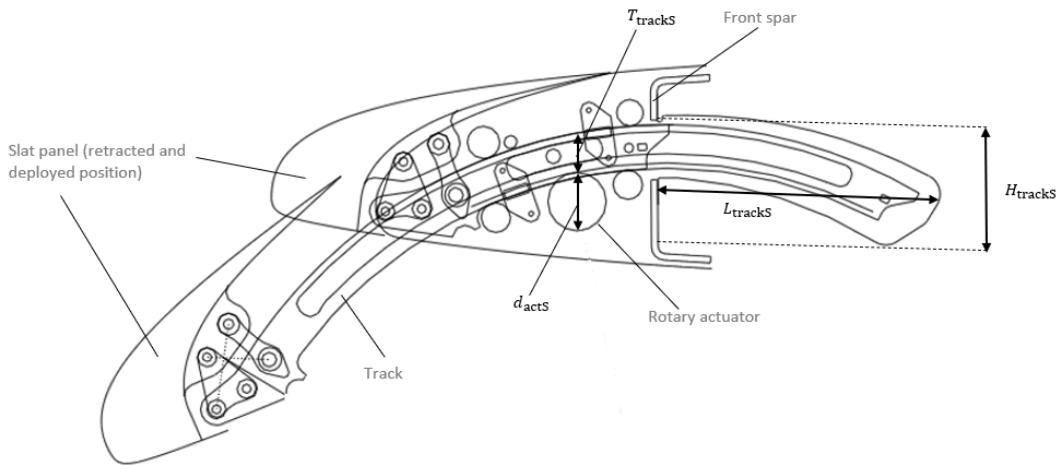


Figure 3.7: Slat system schematic and space envelope parameters of interests, adapted from [4]

The hinge moment for slats system can be calculated using Equation 3.2; it can then be used to correlate with d_{actS} . The slat system track length (L_{trackS}) is defined as the chordwise movement of the track aft of the front spar. Therefore, its length is equal to the movement of the slat in chordwise direction, which can be estimated using the slat chord (C_{slat}) and wing under slat surface (WUSS) chord (C_{WUSS}) as defined in Fig. 3.8. Specifically, considering the deployment kinematics of a typical rotary slat system, the track envelope length is calculated

by

$$L_{\text{trackS}} = (C_{\text{slat}} - C_{\text{WUSS}}) \cos \delta_{\text{max}} . \quad (3.5)$$

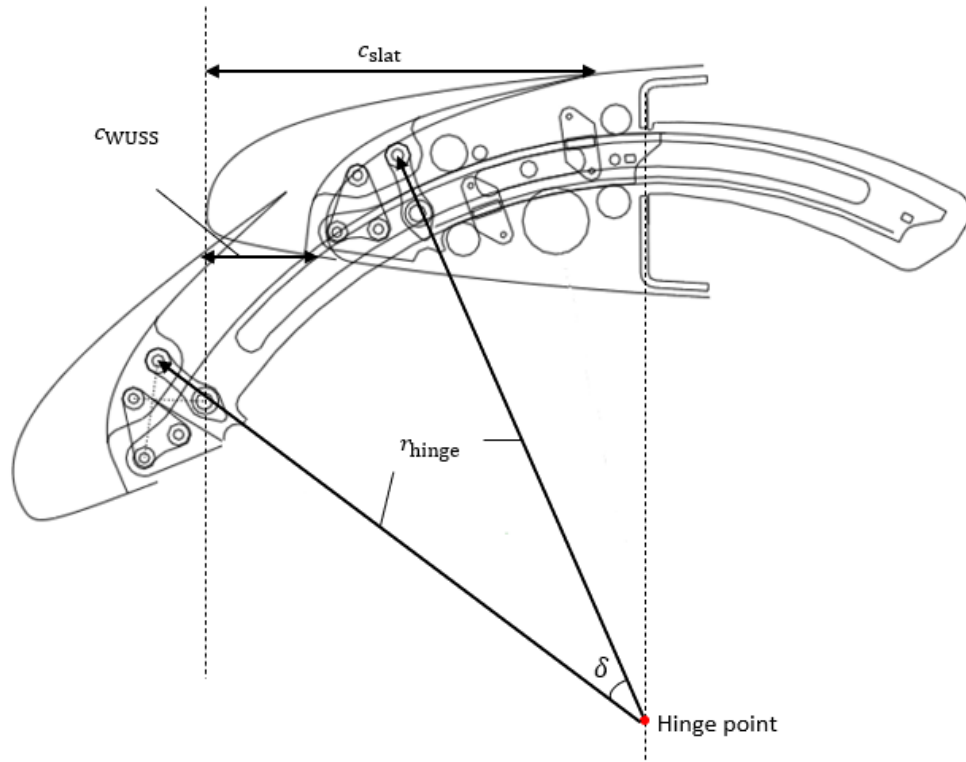


Figure 3.8: Definition of slat chord, WUSS chord, and hinge radius, adapted from [4]

The slat chord and WUSS chord are input to the sizing method, and are expressed as ratio to wing chord at specific airfoil station (slat panel station). The WUSS chord is determined from aircraft anti-icing requirements within aircraft performance module in the existing CMDO framework.

The hinge point is defined as the point where the rotary motion of slat deployment is taken about, and is assumed to be below the front spar for simplicity reason. From Fig. 3.8,

it can be inferred that the hinge radius (r_{hinge}) depends on the required chordwise motion of the slat, which is the track envelope length as previously determined, and maximum deployment angle. After trial and error, the correlation with least R^2 is found to be

$$r_{\text{hinge}} \propto \frac{L_{\text{trackS}}}{\delta_{\text{max}}}.$$

A correlation has also been found between the track height and the estimated slat travel,

$$H_{\text{trackS}} \propto r_{\text{hinge}} \delta_{\text{max}}.$$

A reasonable engineering intuition is to relate track thickness to slats system structural strength, which is then demanded by the aerodynamic load that slat panel is subject to. After experiments with existing aircraft database, it is found that a correlation between thickness and slat panel area yields highest accuracy. Therefore, track thickness, envelope height, and length can now be predicted in a similar manner as in Fig. 3.2. Since the retracted slat system is fully enclosed within airfoil and therefore eliminate the design of fairing like in flap system, sizing of track envelope width becomes unmotivated as its purpose is for fairing wetted area calculation.

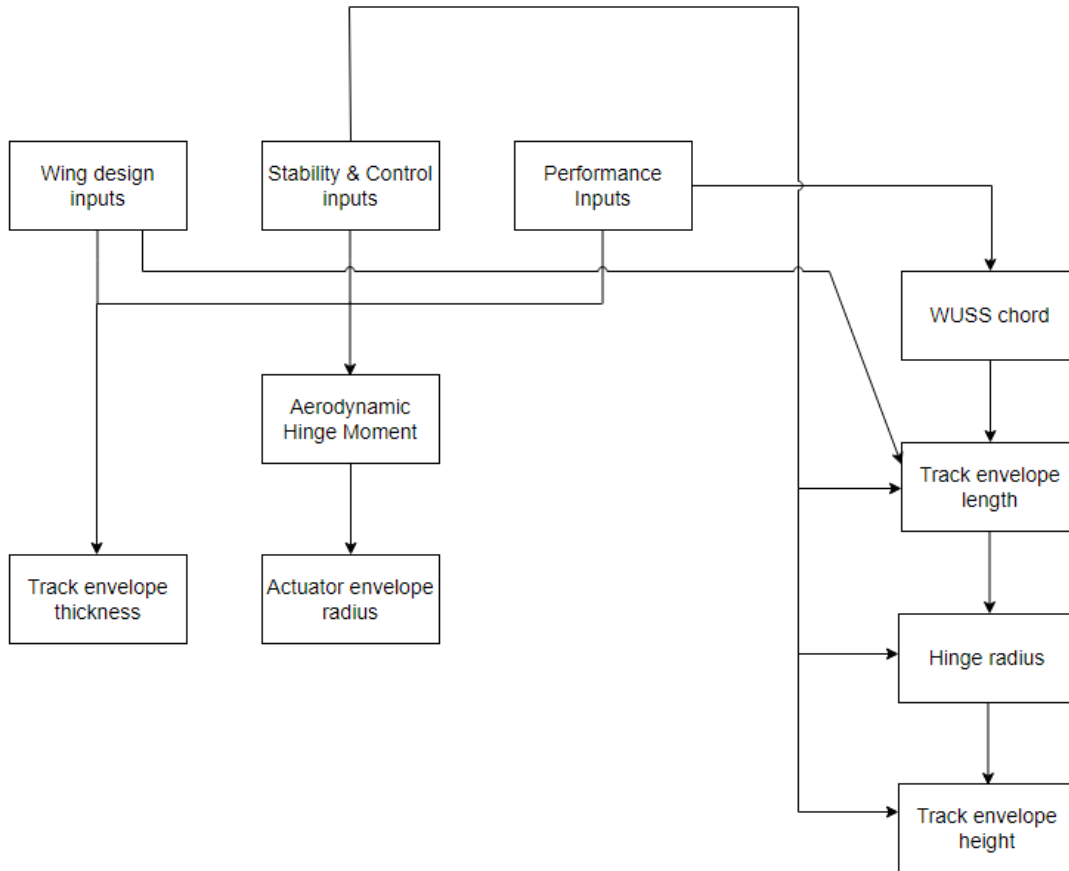


Figure 3.9: High-level diagram of slat system sizing method

3.3 System Envelope Sizing Method for Spoilers

The first step towards method development is to investigate different types of spoiler actuation system mounting. Four main types are identified as shown in Fig. 3.10. Amongst the identified mounting types only pin-to-pin and trunion mounts are used in spoiler actuation systems of the considered aircraft database. The trunion mount is the only type included in this work since it requires less space than pin-to-pin and and it is the mounting

type used mostly in the aircraft database. In addition, since commonality between each type of spoiler has been a common practice in this system's design [70], a common actuation system is assumed for multi-function spoilers (MFS) and for ground spoilers (GS). An example of actuator space envelope definition is shown in Fig. 3.11. OD_{SP} and ID_{SP} are outer and inner diameter of spoiler actuator cylinder, respectively. The space envelope of spoiler FCAS is described by actuator length L_{actSP} , height H_{actSP} , and width W_{actSP} .

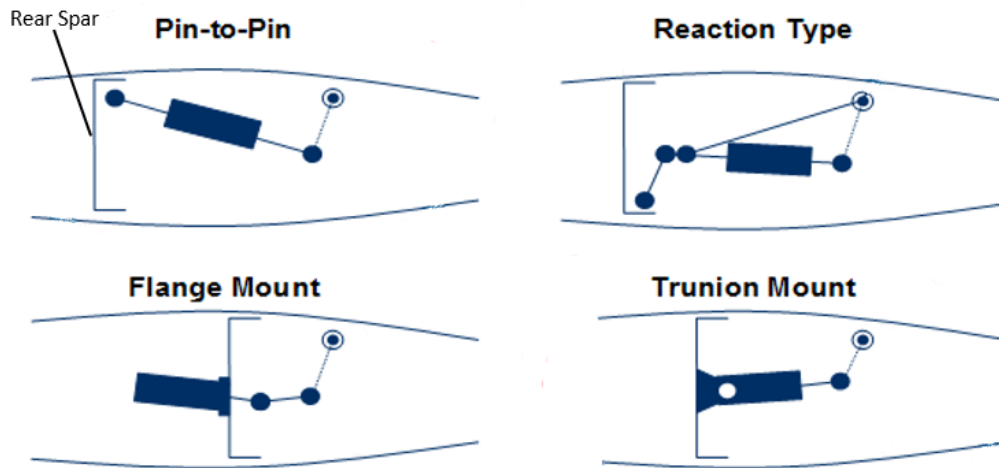


Figure 3.10: Different types of spoiler actuator mountings

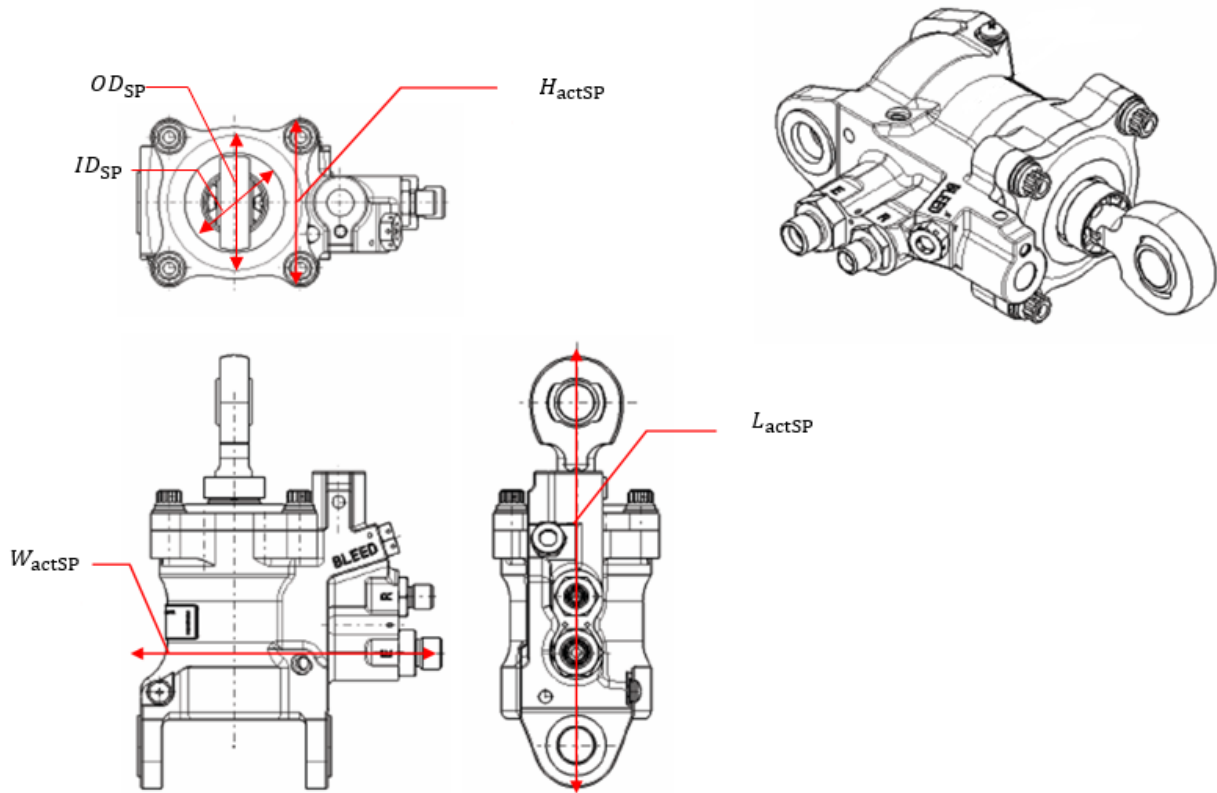


Figure 3.11: Example of space envelope definition for a common spoiler actuator

The first part of the sizing process is to determine the hinge moment from the spoiler control surface. Equation 3.2 can be used to estimate the MFS hinge moment. For ground spoilers, due to the difference in working condition, the V_{fe}^2 term is replaced by aircraft reference approach speed (V_{ref}^2), which is an aircraft-level design specification. The next step in this sizing process is to estimate the horn radius (r_{horn}), which is the moment arm associated with hinge moment. Estimation of horn radius requires a detailed definition of spoilers and flaps' installation, since they are both installed aft of rear spar. As shown in

Fig. 3.12, the horn radius can be calculated by

$$r_{\text{horn}} = T_{W@HL} - T_{F@HL} - D_{HL-uOML}, \quad (3.6)$$

where $T_{W@HL}$ and $T_{F@HL}$ are wing and flap thickness at hinge line, respectively. The

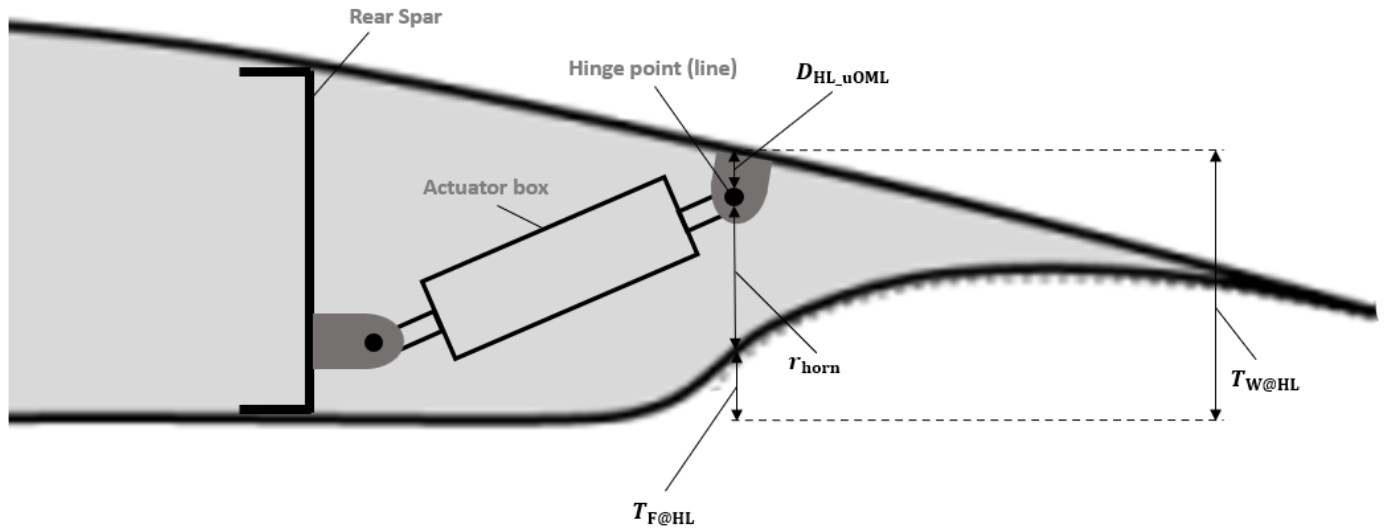


Figure 3.12: System installation schematic for horn radius estimation

distance from the hinge line to the upper outer mold line (OML) $D_{HL-uOML}$ is approximated as 0.9" from observation of aircraft data in this work. At this stage, the aerodynamic load on spoiler actuator (F_{aero}) can be obtained as

$$F_{\text{aero}} = \frac{M_H}{r_{\text{horn}}} f_{\text{safety}}, \quad (3.7)$$

where f_{safety} is a safety margin selected to be 1.2 after consultation with industrial specialists.

The actuator load is the driving factor for the piston area and therefore the inner diameter of the actuator cylinder (as shown in Fig. 3.11). As a result, the cylinder inner diameter can be approximated using its correlation with actuator load. The outer diameter can then

be obtained by finding an average ratio between inner and outer diameters from aircraft database using the proportionality relations

$$ID_{SP} \propto F_{aero} \text{ and}$$

$$OD_{SP} \propto ID_{SP} .$$

Finally, the cylinder outer diameter is used to predict the spoiler actuation system envelope using the proportionality relations

$$L_{actSP}, H_{actSP}, W_{actSP} \propto OD_{SP} .$$

The envelope prediction method for the spoiler system is summarized in Fig. 3.13.

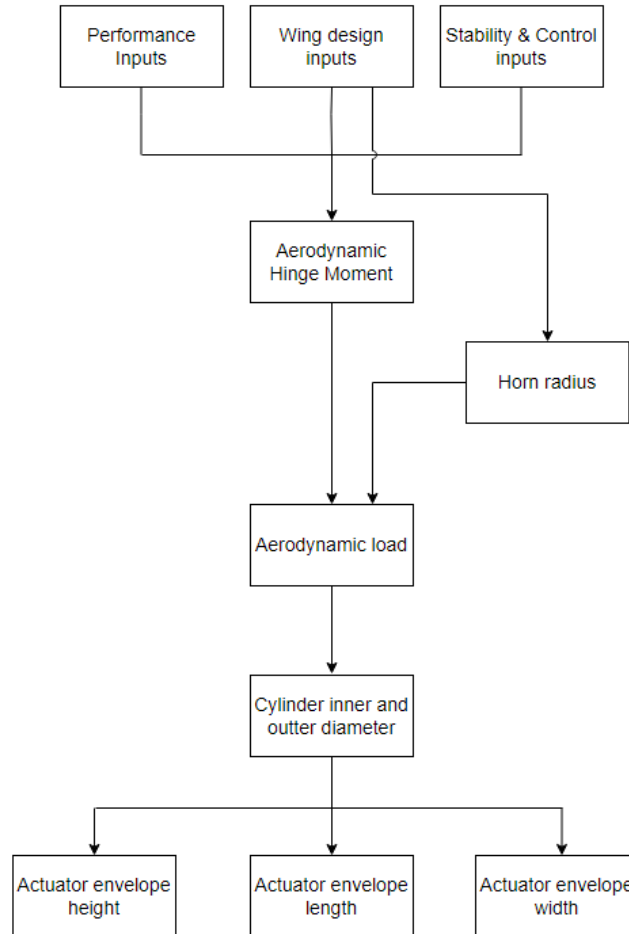


Figure 3.13: High-level diagram of spoiler system sizing method

3.4 System Envelope Sizing Method for Primary Flight Controls

The sizing methods for actuation systems of primary flight controls (PFC), namely rudder, elevator, and aileron, are considered as an ensemble. This is because primary control actuation systems share similarities in

- Deployment mechanism: The actuators, or primary control units (PCUs) for primary flight controls in the scope of this work are all of linear type, which works by linearly moving the hydraulic piston - cylinder rod - lever arm assembly to realize control surface deployment motion. Contrary to linear actuator is rotary vane actuator, which is much less commonly seen in current flight control actuation designs. A graphic illustration for both actuator types is provided in Fig. 3.14.
- System installation: All actuation systems are installed in trailing edge portion of the wing, due to the working nature of primary flight control surfaces; primary flight control PCUs are all installed in between rear and front spar for all aircraft configurations considered in this work. Finally, all aileron are designed without fairings (unlike flaps), which results in a similar process as that for the design of the elevator and the rudder.

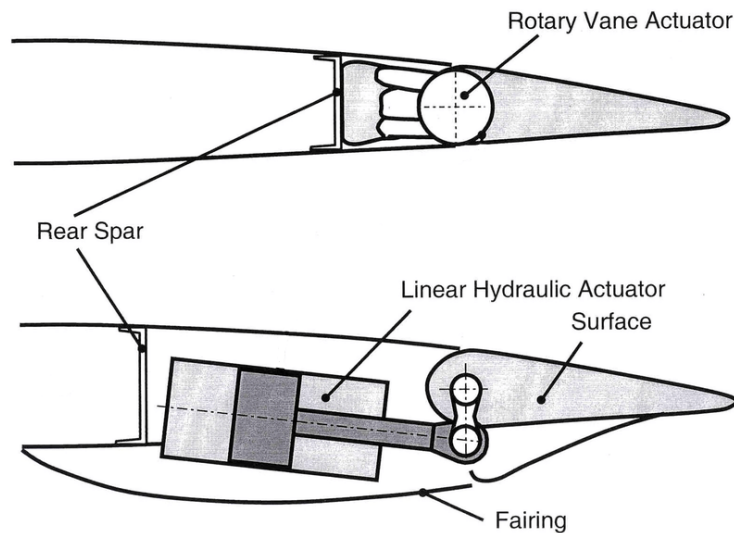


Figure 3.14: Example of linear and rotary vane actuators for primary flight controls [5]

Apart from these similarities, the PCU box of primary flight controls can be classified based on the difference in aircraft control configuration: Hydro-mechanical actuators (HMAs) for conventional fly-by-cable aircraft, and electrohydrostatic actuators (EHSAs) for more electric fly-by-wire aircraft. An HMA PCU box generally occupies a larger envelope than that of EHSA, due to the extra weight and volume of steel cables. However, the diameter of EHSA hydraulic rod is larger due to the existence of a linear variable differential transformer (LVDT), which is an electrically powered transformer used for measuring linear displacement that is installed inside the inner hollow part of EHSA hydraulic rod [71].

A schematic for the actuation system configuration of interest in this work is shown in Fig. 3.15. The diagram is simplified and does not contain detailed components of EHSA or HMA actuators. The envelope parameters of interests include height, length, and width, while the spanwise parameter is not shown on the diagram.

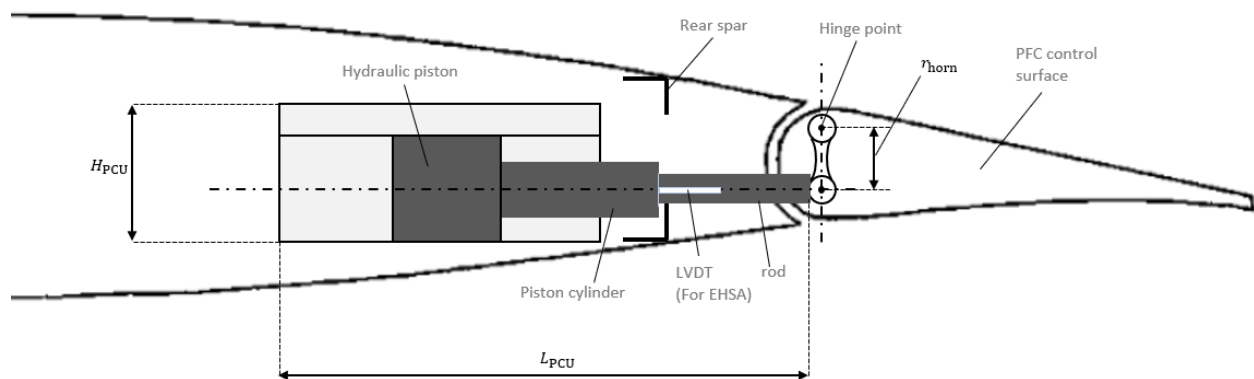


Figure 3.15: PFC system schematic and space envelope parameters of interests

To estimate the hinge moment for PFC surface, Equation 3.2 is reformulated as:

$$M_H = A_{cs} \cdot C_{cs} \cdot M_{OM}^2, \quad (3.8)$$

where M_{OM} is the aircraft maximum operating mach number. This formulation eliminates the usage of δ_{max} and is empirically found to be more accurate than Equation 3.2 for a PFC system.

Another important intermediate parameter is the horn radius (r_{horn}), which is the lever arm between the control surface pivot point (hinge point) and the hydraulic cylinder rod. To achieve a design without blister or fairing, the horn radius has to be constrained by the rear spar height. Through analysis of aircraft database, a linear correlation between the horn radius and the rear spar height has been found for the aileron and the elevator. Since the rudder system's hinge point is centered on the control surface cross section instead of close to the upper surface as in Fig. 3.15, a separate correlation formulation with rear spar height for rudder is established to yield a lower estimation of horn radius.

With the hinge moment and the horn radius calculated, the actuator aerodynamic load can now be obtained using Equation 3.7. The required piston area can then be obtained as

$$A_{piston} = \frac{F_{aero}}{P_{system} - P_{return}}, \quad (3.9)$$

where $P_{system} = 3000 \text{ psi}$ and $P_{return} = 160 \text{ psi}$ based on the input from an aircraft manufacturer. The obtained piston area can be used to calculate the diameter of the piston cylinder. The cylinder is a hollow design for weight saving purpose, and its inner diameter

can be calculated by

$$ID_{\text{PFC}} = \sqrt{\frac{\pi}{4} \cdot A_{\text{piston}} + d_{\text{rod}}^2}, \quad (3.10)$$

where d_{rod} is the diameter of the rod connected to the piston cylinder. An empirical approach can be applied to correlate the cylinder outer diameter (OD_{PFC}) to cylinder inner diameter (ID_{PFC}) using aircraft database. In this case the relationship found is

$$OD_{\text{PFC}} = 1.5 \cdot ID_{\text{PFC}}. \quad (3.11)$$

The rod is also of hollow design for EHSA, in order for the LVDT to be installed as previously mentioned. The required cross sectional area is defined through stress analysis (tensional stress and buckling analysis), which results in the required stress (σ_{req}) that the rod is anticipated to be subject to. The expression of rod diameter can then be analytically obtained by

$$d_{\text{rod}} = \sqrt{\frac{\pi}{4} \cdot \frac{F_{\text{aero}}}{\sigma_{\text{req}}} + D_{\text{LVDT}}^2}, \quad (3.12)$$

where F_{aero} is evaluated using Equation 3.7. D_{LVDT} is the inner diameter of the rod cross section equals to 0.75". In the case of HMA, the rod is solid and thus $D_{\text{LVDT}} = 0$. For the conceptual design phase, the required stress on PCU rod (σ_{req}) is given by the structure team as a fixed value (31000 lb/in^2 for HMA, 24600 lb/in^2 for EHSA), instead of being computed.

The piston cylinder outer diameter can be determined using Equations 3.11, 3.10, and 3.12. The PCU space envelope height is found to be highly correlated with cylinder outer diameter through aircraft database analysis.

Due to the working mechanism of the linear actuator, the PCU envelope length depends

on the required piston stroke, which is a function of the total control surface travel and the horn radius. It would be intuitive to use the piston cylinder length as a driving factor to size envelope length, but due to the lack of cylinder length data in the gathered aircraft drawing database such a correlation is not considered here. Nevertheless, the following correlation yields adequate estimation from a statistical point of view (relatively low R^2 value):

$$L_{PCU} \propto \delta_{max} r_{horn} ,$$

where δ_{max} is the total control surface travel.

The sizing method for PCU envelope width is separated between HMA and EHSA, due to their work load difference as mentioned previously in this section. As the case of flaps, spanwise parameters are generally estimated using the correlation with aerodynamic load. For primary flight controls the correlation with actuator load yields better accuracy:

$$W_{PCU} \propto F_{aero} .$$

Correlation formulation for HMA and EHSA systems are developed separately. Fig. 3.16 provides a schematic of the developed primary flight control system envelope prediction method.

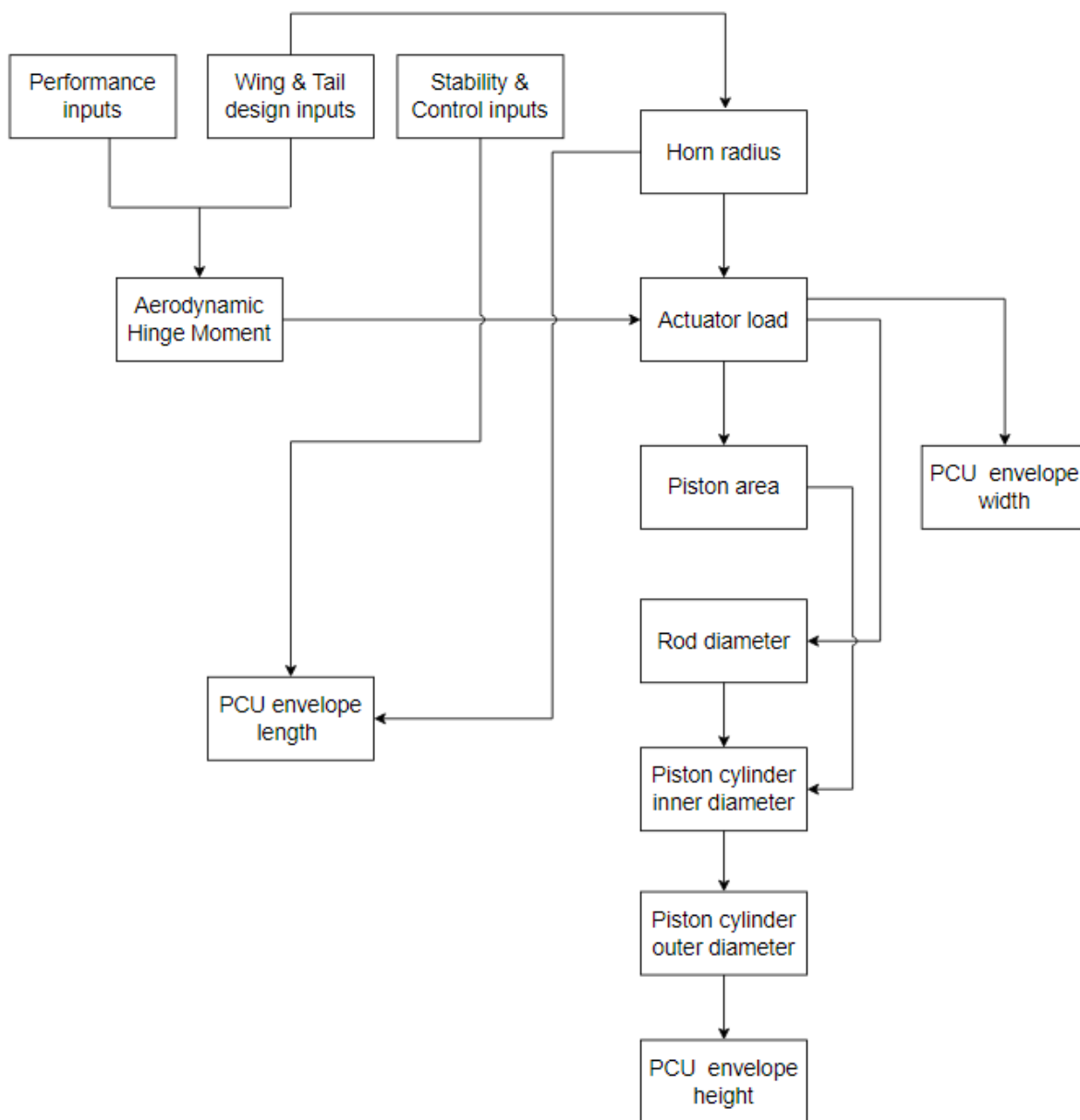


Figure 3.16: High level diagram of primary flight control system sizing method

3.5 Model Validation and Uncertainty Quantification

Although accuracy is considered mainly during the prediction model development process, a comprehensive method validation for all flight control actuation systems is considered after the models are developed. The aircraft database included in this work contains reference parameters (intermediate parameters and space envelope parameters; availability of these parameters varies for each aircraft in the database), and can be used to compare against estimated parameters from the models. In case the mean error is high ($>20\%$), a correction factor is manually added to the calculation of the corresponding parameter. The value of the correction factor is determined by the average of $\frac{\text{Estimated parameter value}}{\text{Reference parameter value}}$. An example of such validation applying to hinge moment estimation of primary flight control system is shown in Fig. 3.17. It is noted that the PFC hinge moment estimation is less accurate for rudder systems, which is discussed further in Section 6.

Due to the estimation nature of the model, uncertainty exists. From a systems integration point of view, it is of interest to investigate the influence of uncertainties on the final predicted space envelope results in order to obtain the required design margin during the early design stage. The first step is to identify the parameters with uncertainty. Since most procedures of the prediction methods are uncertain and since that uncertainty propagates through the prediction process, it is more efficient to consider only low-level parameters as random. In the example case of aileron (primary flight control system), the assumed random variables are aerodynamic hinge moment and horn radius. In addition, an intermediate parameter,

rod diameter, is included due to its high level of uncertainty.

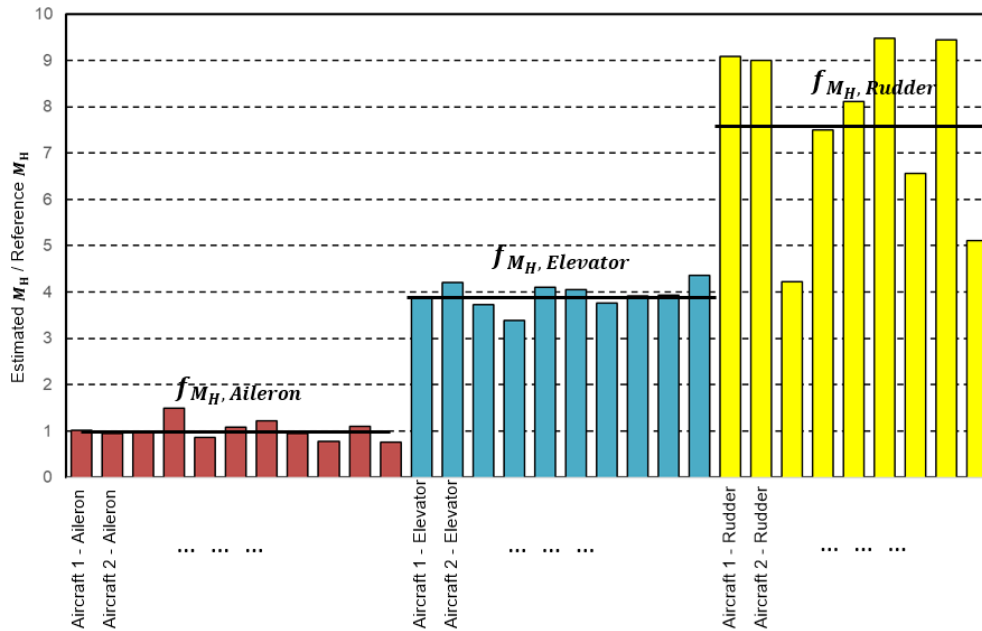


Figure 3.17: Example of determining correction factor value for PFC hinge moment estimation

The next step is to model the identified random variables. Considering the amount of data provided in the database, it is more realistic to assume linear (triangular) distributions for the random variables, with mean, lower and upper limits of error calculated at the validation step. Random variable modelling is shown graphically in Fig. 3.18.

Monte-Carlo simulation is conducted to obtain system envelope distributions for a given set of inputs. The results are presented in Fig. 3.19 for the example case of aileron PCU envelope height estimation. The useful lessons obtained by these results include:

- For a high level of confidence, the range of predicted result will fall between 6.33” and

6.54” for the aileron PCU envelope height.

- The value of the system space envelope is highly unlikely to exceed 6.62” of aileron PCU envelope height.
- The likelihood to raise a flag during system integration is not large. For example, with a sparwise space constraint considering margin to be 6.55”, the probability of aileron PCU sparwise integration failure is 8%.

In general, the results of this uncertainty quantification make the prediction model more robust in supporting decision making process during the conceptual design phase.

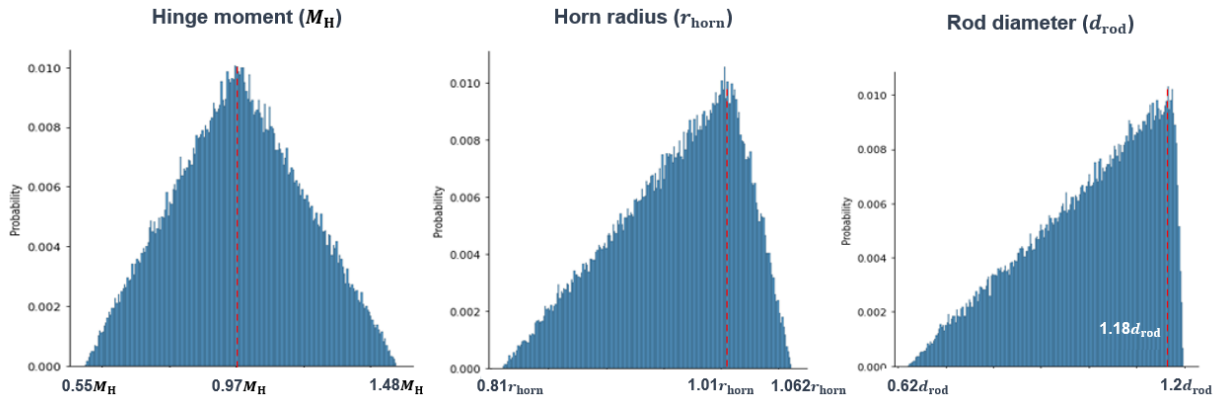


Figure 3.18: Random variable modelling for Aileron actuation system space envelope estimation

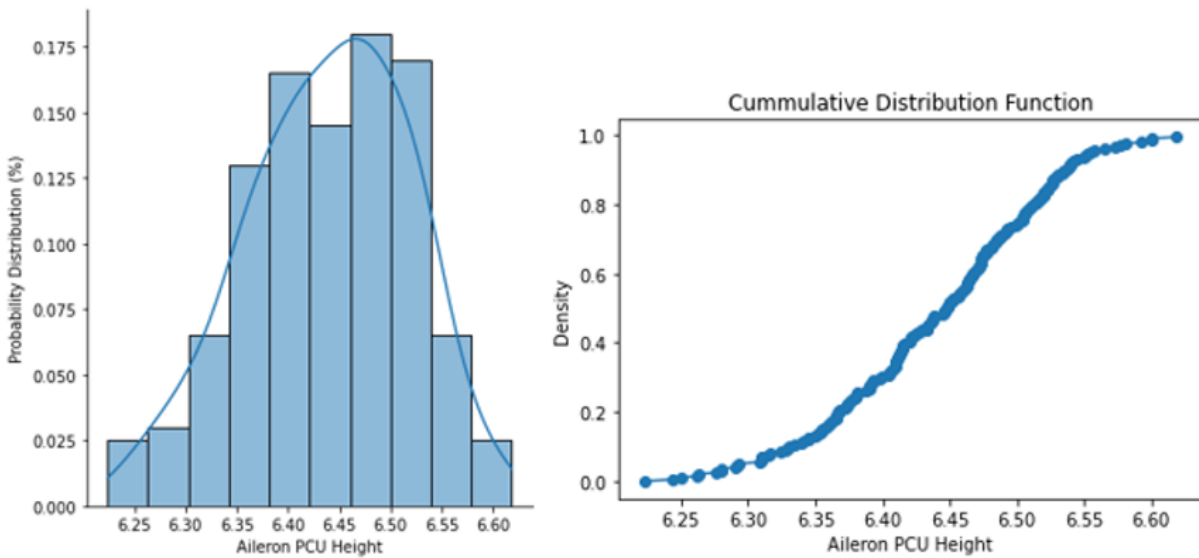


Figure 3.19: Monte-Carlo simulation of aileron PCU envelope height distribution

Chapter 4

Aircraft CMDO Workflow Overview

4.1 Aircraft CMDO Environment and Architecture

The developed FCAS space envelope prediction models are integrated in an existing CMDO framework, which is a monolithic multidisciplinary design feasible (MDF) architecture shown in Fig. 4.1. The CMDO framework is implemented as a workflow in Isight [72]. Isight is a tool-integration, design-optimization software developed and distributed by Dassault Systems. The objective of the MDO problem is to minimize the maximum take-off weight (MTOW) of the aircraft (under a fixed payload, this is equivalent to minimizing aircraft structural weight), since it serves as a proxy of several disciplines including cost and climate impact through fuel burn. For this reason, an economics discipline is not included in this study. Note that aircraft structural strength analysis is not included at the low-fidelity

CMDO stage; a fixed wing airfoil geometry is used throughout the aerodynamic module (airfoil shape optimization is not considered in CMDO).

The constraints of the MDO problem include

- Aircraft performance requirements: balanced field length, maximum range, initial cruise altitude, approach speed, etc. This is discussed in [73–75].
- Stability and control requirements: center of gravity (CoG) limits, static margins about Fwd/Mid/Aft CoG during cruise, climb and approach. This is discussed in [76].
- Landing gear integration requirements: landing gear geometrical constraints considering retraction kinematics, ground handling constraints. This is discussed in [55, 56].
- FCASs integration requirements: FCASs envelope geometrical constraints obtained after post-processing of FCASs sizing model output. This will be further discussed in Section 4.3.

The design variables of the MDO problem include

- Wing-related: area, taper ratio, thickness, sweep, span.
- FCASs-related: number of actuators, number of control surfaces and panels, PCU technology, system deployment mechanism.
- Engine-related: engine scaling factor.

In this study the engine scaling factor was kept constant. Such an assumption is common in aircraft conceptual design due to the presence of a pre-existing engine platform. FCASs variables are also fixed since these are assumed as pre-defined engineering choices.

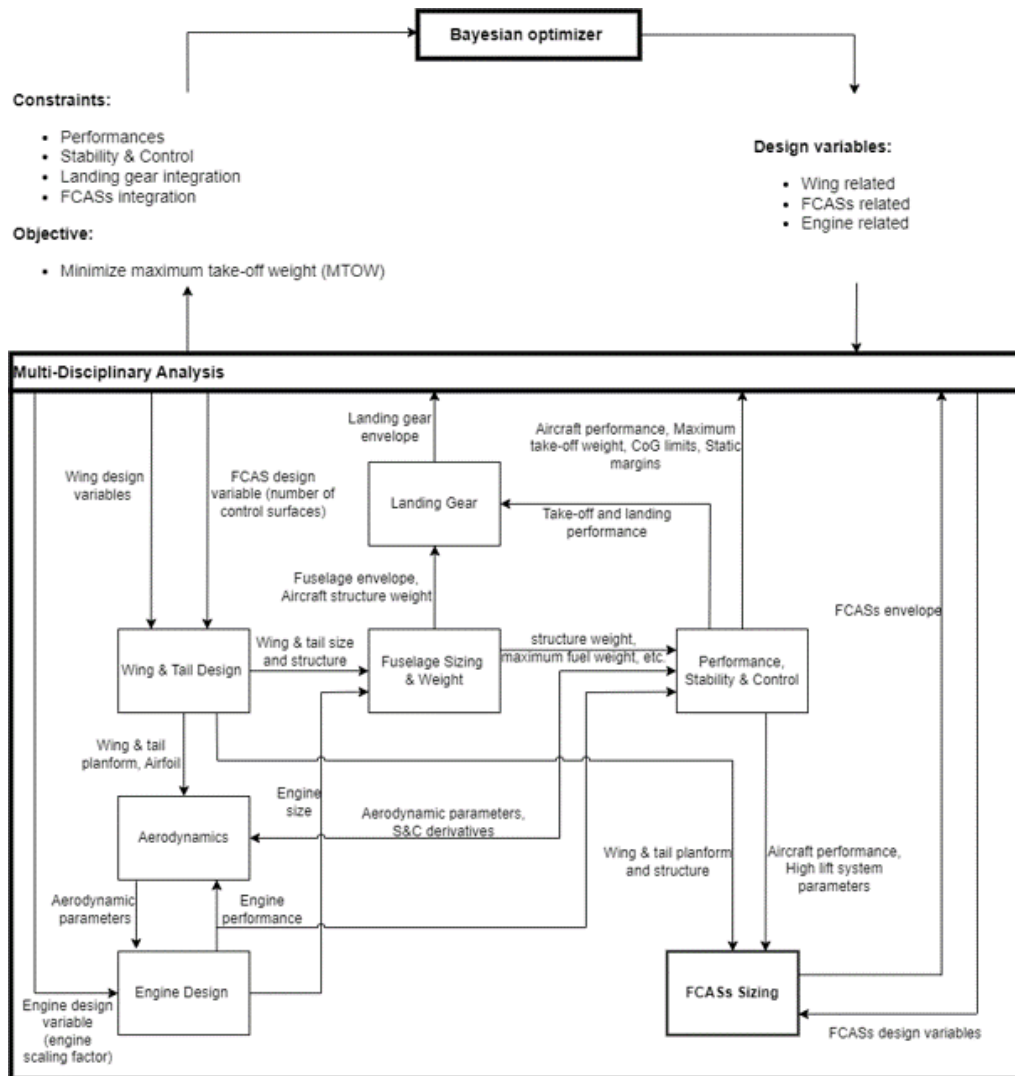


Figure 4.1: Schematic of aircraft MDO problem with integration of FCASs sizing discipline

The variables linking disciplines include:

- Subsystems weight (structure, fuel, aircraft systems, wing, engine, miscellaneous)
- Engine characteristics (bleed characteristics, fuel consumption, power rating)
- Wing and tail planform (control surfaces' and panels' surface area and chord length)
- Wing and tail structure (FCASs' and control surfaces' spanwise and chordwise location, control surfaces' and panels' thickness, spars' location and length)
- Aerodynamics parameters (drag, lift, buffet, aerodynamic coefficients)
- High lift system parameters (control surfaces' total travel, panels' maximum deflection.)

The optimizer of the MDO formulation in Isight calls different disciplines using a sequential approach. The sequence definition of discipline evaluation is shown in Fig. 4.2. The FCAS sizing module is added to the end of existing sequence since it requires input from multiple modules.

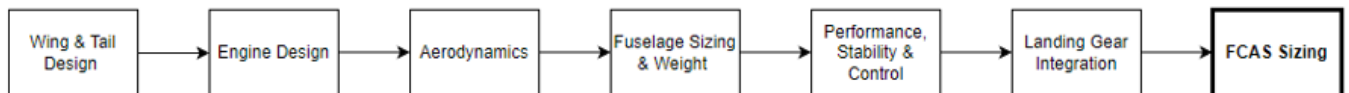


Figure 4.2: Sequence of discipline evaluation within current MDO formulation with chosen sequence addition of FCASs Sizing

4.2 Aircraft CMDO Optimizer

In this study, a constrained Bayesian optimization (CBO) framework is used to solve the MDO problem [6]. The CBO framework is a form of surrogate-based optimization, which uses surrogate model (Kriging for CBO) to compute objective and constraint function values [77]. A schematic of the surrogate-based optimization workflow is shown in Fig. 4.3.

MDO Problem Formation:

$$\begin{aligned} & \min_{x \in \mathbb{R}^d} \hat{y}(x) \\ & \text{subject to } \hat{c}_i(x) \leq 0 \quad (i = 1, \dots, m) \end{aligned}$$

Optimizer:

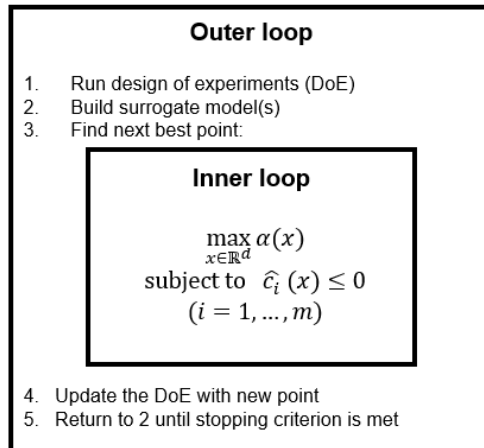


Figure 4.3: Overview of the general surrogate-based optimization algorithm, adapted from [6]

In Figure 4.3, x represents the design variables, $\hat{y}(x)$ and $\hat{c}_i(x)$ represent objective and constraint functions computed by surrogate models, and m denotes number of constraints. The surrogate model is trained using data obtained from a design of experiments (DoE). To determine the next point to be evaluated by the high-fidelity model to adapt the

surrogate model with the goal of improving its predictive capability, an infill criterion $\alpha(x)$ is maximized. This iterative process is terminated when a pre-defined maximum number of iterations is reached. The solution of the CBO is the point with the minimal feasible value of the objective function. Fig. 4.4 presents an example of the one-step selection of the next best DoE, and it can be seen that the surrogate model is further adapted to better match the objective function.

Within this context, an efficient global optimization (EGO) algorithm is developed using expected improvement (EI) derived from likelihood maximization as infill criterion. EGO is modified into super EGO (SEGO) with the usage of Watson and Barnes infill criterion [78], which introduces subtraction of mean value of the Kriging surrogate from EI. A detailed discussion of EGO and SEGO algorithm can be found in [79, 80].

To mitigate the objective and constraint functions' non-linearity that exists in most industrial engineering problems, a mixture of experts (MOE) technique is added to SEGO to develop the SEGOMOE algorithm. The key idea is to use different local approximation models, including Kriging, Kriging with partial least squares (KPLS), polynomial regression, and radial basis functions to construct the surrogate models. A detailed discussion of the SEGOMOE algorithm developed by ONERA as a python tool-box is available in [81]. It comes with an Isight interface and is adopted as the optimizer in this study.

In this study, a SEGOMOE-based optimizer is used to solve the aircraft MDO problem with a given set of constraints. In addition, a linear sensitivity analysis of the objective

function to the constraints is pursued. In particular, it is of interest to investigate the feasibility of performing such sensitivity analysis through a machine learning (ML)-based approach considering the high computational cost of solving the MDO problem. To develop such approach, a standalone SEGOMOE ML model is trained with a set of constraint values obtained from CMDO loop evaluations. The model is then able to make predictions on objective function with a desired set of constraint values as input. Details and preliminary results generated from the developed ML-based methodology is recorded in Section 5.3.

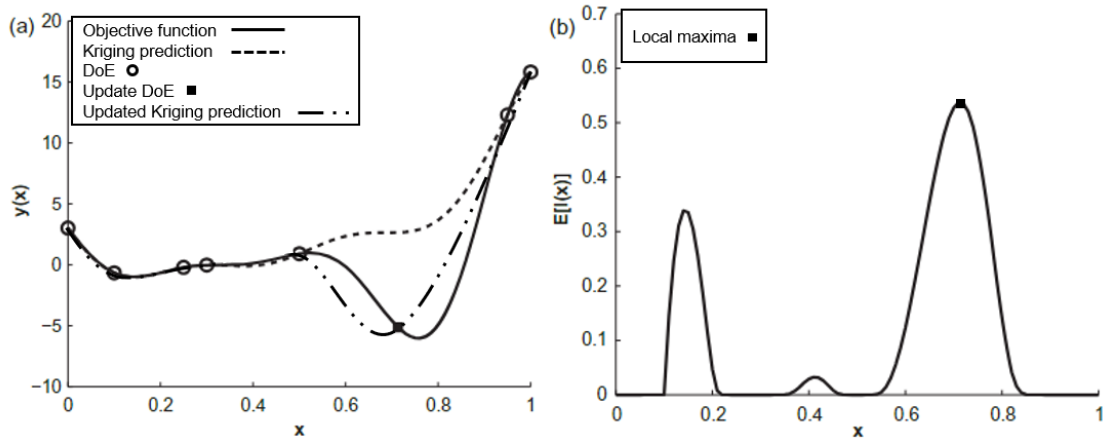


Figure 4.4: Illustration of one step DoE enrichment and surrogate model adaptation on an example of one-dimensional Forrester function. (a) Kriging prediction and the location of the next update DoE, (b) Infill criterion (Expected Improvement, EI), adapted from [7]

4.3 Integrated FCASs Space Envelope Prediction Model within CMDO

A data flow schematic of the FCASs sizing module is shown in Fig. 4.5 to visualize the dependencies arising from integrating the module into the CMDO environment. It also contains post-processing, which takes FCASs sizing module output and generates parameters that were treated as newly-introduced constraints. These constraints include:

- Sparwise clearance related constraints: a design margin must be kept in the sparwise direction (thickness direction). This is calculated as the difference between height of actuator/PCU/track and the spar height at the spanwise location of actuation system attachment.
- Aileron PCU and slat track chordwise gap: A sufficient chordwise gap must be kept to allow for other wing structures (pneumatic system, fuel tank, etc.) to be installed. This is calculated as the distance between rear and front spar subtracted by the sum of slat track and aileron PCU length. This is considered at spanwise locations where slat and aileron actuation systems are both present.
- Spoiler actuator area ratio: This is the spoiler actuator area divided by the available area aft of rear spar. Typically, a less than 50% area ratio is sought.
- Spoiler actuator chordwise clearance: a design margin must be kept between the spoiler

actuator length and the chordwise space aft of rear spar. As in Fig. 3.12, the actuator length sought here is the projection of envelope length on the chordwise direction, and can be calculated using known horn radius.

- Flap track fairing wetted area ratio: This is considered as the best criterion for flap system space envelope constraints, since the system is implemented inside the wing fairing instead of wing. The wetted area must be controlled for aerodynamic reasons, and it is evaluated as a ratio to wing planform area.

Chordwise clearance constraints for PFC actuation system are not considered, since they are implemented in between rear and front spar, where chordwise space is considered ample. A similar argument can be stated for slat systems, whose track length envelop is measured aft of front spar as in Fig. 3.7. The spoiler actuator sparwise clearance is not considered either, since its sparwise location is constrained by the distance from the hinge line to the upper outer mold line (OML) ($D_{HL-uOML}$) as in Fig. 3.12.

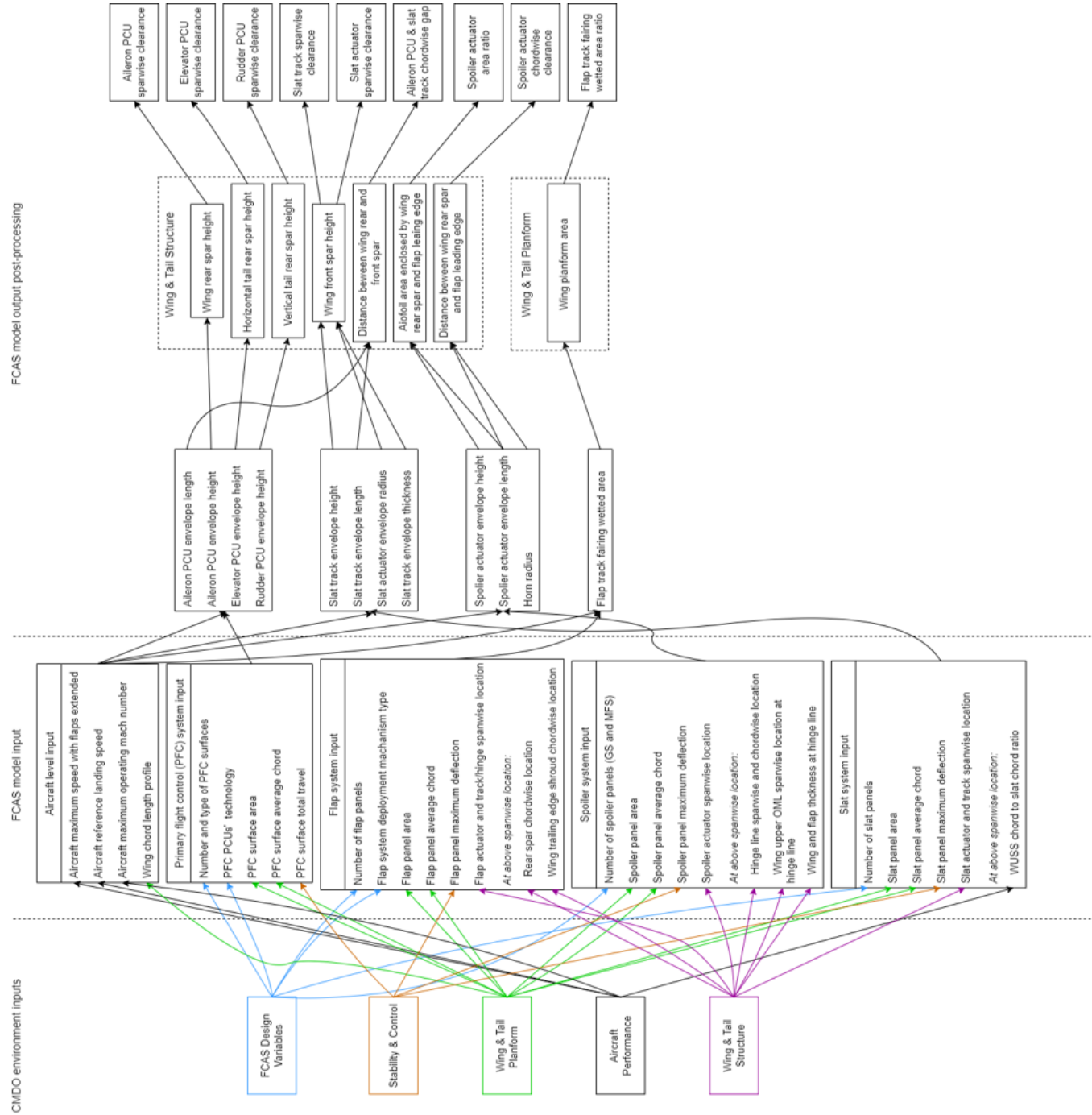


Figure 4.5: Schematic showing data-flow of FCASs sizing module within CMDO environment and post-processing

Chapter 5

Numerical Investigation and Results

5.1 Comparison of Obtained Designs

After the integration of the FCASs space envelope sizing model into the CMDO environment, the first investigation is to execute the updated optimization workflow and report the results in comparison with the ones obtained with no FCASs space envelope constraints. A business jet aircraft with aft mounted engines and a T-tail design is adopted as the reference aircraft, and a common starting design is used for both test cases. The values of each FCAS space envelope constraint are carefully determined to ensure it satisfies product development requirements from a system integration point of view.

For both test cases, the size of initial DoEs is set equal to 50, and the maximum number of evaluations is set equal to 300 (i.e., a total of 350 evaluations). Both test cases converged

to the same objective value within the allocated number of evaluations. The number of feasible runs for the test cases with and without FCASs space envelope constraints are 89 and 117, respectively. A selected set of parameters comparing optimization results with and without FCASs constraints are shown in Table 5.1.

Table 5.1: Variance of optimization results obtained with FCASs constraints comparing to the results obtained without FCASs constraints

Wing span (variable)	Wing area (variable)	Wing average thickness (variable)	Horizontal tail span (variable)	Horizontal tail average thickness (variable)	Range (output)	Take-off weight (objective)
+0.1%	+2.1%	+6.9%	0.0%	+5.8%	-2.1%	+1.2%

It is noted that the wing and tail span remain similar, since the FCASs sizing module does not introduce spanwise constraints. The increase in wing planform area (2.1%) is caused by the increase in wing mean chord, which implies that one or all of the wing chordwise constraint(s) is (are) active. The sizing effect is more evident on wing and tail thickness (6.9% and 5.8%), due to the introduced sparwise constraints. The FCASs integration consideration finally leads to an increase in MTOW (1.2%) and decrease in cruise range (2.1%).

The comparison of wing planform design and wing thickness sizing is graphically illustrated in Figure 5.1 and Figure 5.2. Figure 5.3 provides the spanwise location of each FCAS, excluding that of flaps since it is housed inside wing fairing instead of wing. Figure 5.3 also illustrates the location of wing airfoil selected in Figure 5.2.

From Figure 5.1, it can be seen that the tail planform design remains similar. It is also noted that the increase in chord length is more evident towards the wingtips, which implies

that the aileron PCU & slat track chordwise gap constraint is active, based on the spanwise location of aileron and outboard (away from wing root) slat FCAS. Both test cases reach maximum wing sweep angle, and considering the lower aspect ratio of the design optimized with FCASs constraint, it is concluded that such design is less aerodynamically efficient and contributes to the decrease in cruise range (-2.1%). Another observation drawn from Figure 5.2 is that the difference in wing thickness is less evident towards the wingtips, which is expected since the wing design module imposes such convergence of thickness towards the tip.

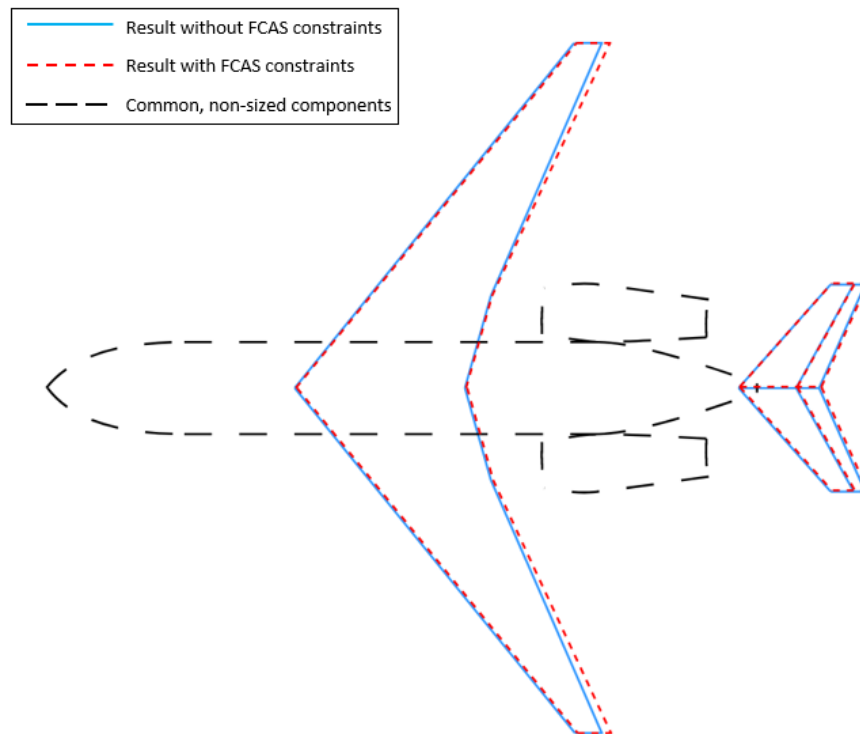


Figure 5.1: Optimal wing and tail planform designs with and without FCASs constraints

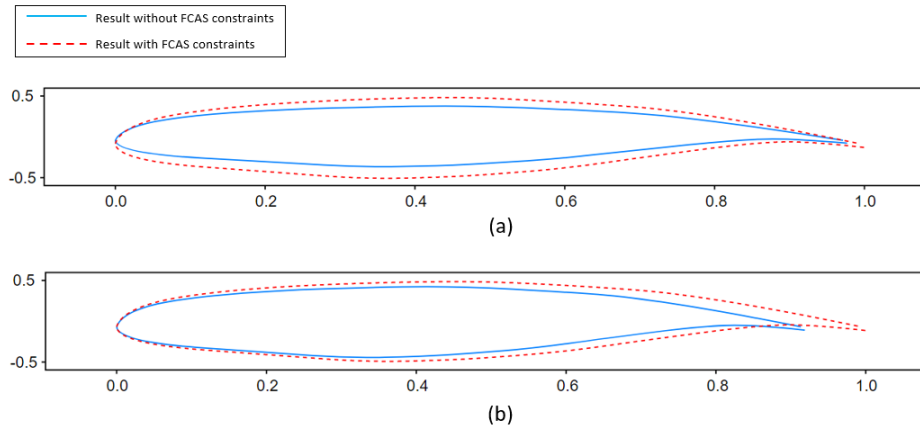


Figure 5.2: Optimal wing airfoil designs with and without FCASs constraints at (a) 57% spanwise location and (b) 89% spanwise location.

A detailed list of the design variables and constraints of the two test cases is provided in Table 5.2. The engine scaling factor is fixed at 1 and is therefore excluded in Table 5.2. The number of actuators/PCUs is assumed to be the same as the number of corresponding control surfaces (i.e. one actuator/PCU per control surface assumed). The identified active constraints include:

- The reference landing speed (V_{ref}) is active only in the test case with FCASs constraints. This is led by the increase in MTOW.
- Landing gear tip over angle and landing gear skin clearance, which depends on the positioning of the main landing gear relative to the wing and aircraft CoG [56].
- Aileron and elevator PCU sparwise clearance, which contributes to the increase in wing and horizontal tail average thickness. It is noted that the rudder PCU sparwise

clearance constraint is not active, which results in the vertical tail average thickness being similar to the reference test case.

- Inboard slat actuator sparwise clearance, which contributes to increase in wing thickness. This constraint for the outboard slat panel is not active due to the increase in wing thickness caused by aileron actuator. In addition, it can be inferred that the envelope height of slat track is smaller than that of slat actuator, since the constraint for the former is not active.
- Aileron PCU & slat track chordwise gap, as previously explained.
- Spoiler actuator area ratio. The activity of this constraint contributes to the increase in wing thickness, given that the spoiler actuator chordwise clearance constraint is not active.

Table 5.2: Comparison of optimization results with and without FCASs constraints

						MDO results	
		Unit	Lower bound	Upper bound	Fixed value	Without FCAS constraints	With FCAS constraints
Wing & tail design variables	Wing span (normalized)	-	0.8	1.2	-	0.99	0.99
	Wing area (normalized)	-	0.8	1.2	-	0.93	0.95
	Wing average thickness to chord ratio	-	0.08	0.16	-	0.117	0.125
	Wing 1/4 chord sweep	degrees	25	35	-	35	35
	Wing trailing edge sweep	degrees	0	25	-	24	25
	Wing taper ratio	-	0.15	0.3	-	0.19	0.22
	Horizontal tail span (normalized)	-	0.8	1.2	-	0.94	0.94
	Horizontal tail area (normalized)	-	0.8	1.2	-	0.96	0.96
	Horizontal tail trailing edge sweep	degrees	15	30	-	30	29.9
	Horizontal tail taper ratio	-	0.25	0.5	-	0.44	0.44
	Horizontal tail average thickness to chord ratio	-	0.08	0.16	-	0.114	0.121
	Vertical tail span (normalized)	-	0.8	1.2	-	0.97	0.97
	Vertical tail area (normalized)	-	0.8	1.2	-	0.95	0.95
	Vertical tail trailing edge sweep	degrees	15	30	-	29.4	29.4
	Vertical tail taper ratio	-	0.3	0.5	-	0.41	0.41
Vertical tail average thickness to chord ratio	-	0.08	0.16	-	0.115	0.116	
FCAS fixed design variables	Number of aileron panel(s) (per side)	-	-	-	1	1	1
	Number of elevator panel(s) (per side)	-	-	-	1	1	1
	Number of rudder panel(s)	-	-	-	1	1	1
	PFC PCU technology	-	-	-	EHSA	N/A	EHSA
	Number of flap panel(s) (per side)	-	-	-	3	3	3
	Flap system deployment mechanism	-	-	-	Fowler type	N/A	Fowler type
	Number of spoiler panel(s) (per side)	-	-	-	2	2	2
	Number of slat panel(s) (per side)	-	-	-	2	2	2
Constraints	Initial climb altitude	ft	40000	-	-	43890	42523
	Balanced field length	ft	-	6000	-	5481	5619
	Reference landing speed	knots	-	125	-	121.7	124.8
	Landing gear tip over angle	degrees	10	-	-	10.1	10.3
	Landing gear skin clearance	inches	1.5	-	-	1.52	1.51
	Static margin during cruise, Mid CoG	% mean chord	0.25	-	-	0.38	0.36
	Static margin during climb, Fwd CoG	% mean chord	0.45	-	-	0.58	0.54
	Aileron PCU sparwise clearance	inches	2	-	-	N/A	2.01
	Elevator PCU sparwise clearance	inches	2	-	-		2.02
	Rudder PCU sparwise clearance	inches	2	-	-		2.25
	Slat track sparwise clearance [1]	inches	2	-	-		3.42
	Slat track sparwise clearance [2]	inches	1.75	-	-		2.95
	Slat actuator sparwise clearance [1]	inches	2	-	-		2
	Slat actuator sparwise clearance [2]	inches	1.75	-	-		2.21
	Aileron PCU & slat track chordwise gap	inches	20	-	-		20
	Spoiler actuator area ratio [1]	-	-	0.4	-		0.39
	Spoiler actuator area ratio [2]	-	-	0.4	-		0.4
	Spoiler actuator chordwise clearance [1]	inches	0.75	-	-	0.89	
	Spoiler actuator chordwise clearance [2]	inches	0.5	-	-	0.81	
	Flap track fairing wetted area ratio	-	-	0.15	-	0.12	

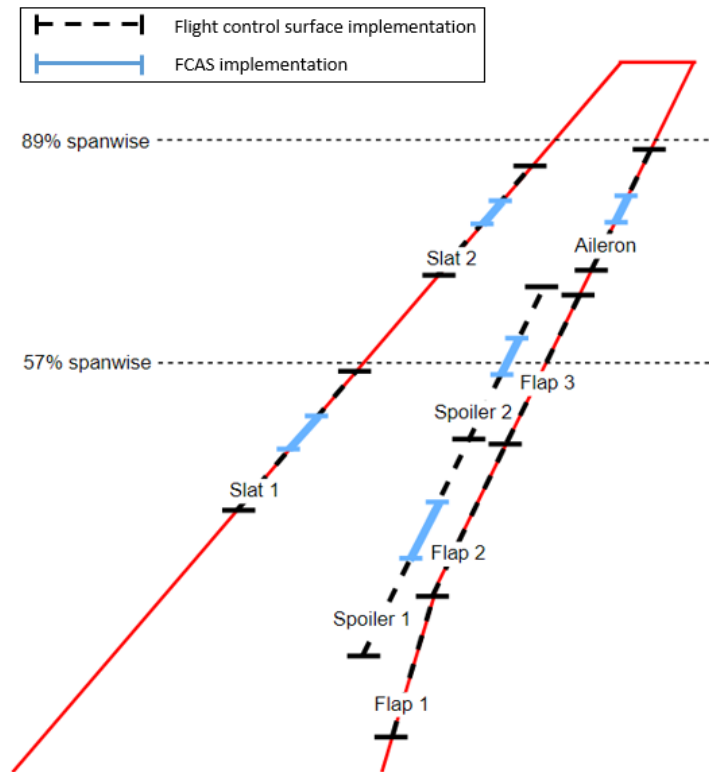


Figure 5.3: Location of flight control surfaces and corresponding FCASs of the optimal aircraft design with FCASs constraints

5.2 Optimal Design Sensitivity Analysis

This section investigates the sensitivity of the objective (MTOW) with respect to the values of the FCASs space envelope constraints. This is done by altering one of the interested constraints by a certain percentage ($\pm 10\%$ in this study) while holding the rest of the CMDO problem formulation unchanged. The constraints of interest in this section are selected to be

the active constraints identified in Section 5.1. Experiments are performed with the value of these constraints taken at 90%, 94%, 98%, 100%, 104%, 108%, and 110% of the reference value. The reference value is taken as the constraint value set up in Section 5.1. The list of constraints investigated and their reference values are summarized in Table 5.3. Note that the outboard spoiler is referred to as multi-functional spoiler (MFS).

Table 5.3: Constraints to be investigated and their corresponding reference value

	Aileron PCU sparwise clearance	MFS actuator area ratio	Elevator PCU sparwise clearance	Aileron PCU & slat track chordwise gap	Inboard slat actuator sparwise clearance
Reference value	≥ 2 inches	$\leq 40\%$	≥ 2 inches	≥ 20 inches	≥ 2 inches

The results of sensitivity analysis are plotted in Figure 5.4 and tabulated in Table 5.4.

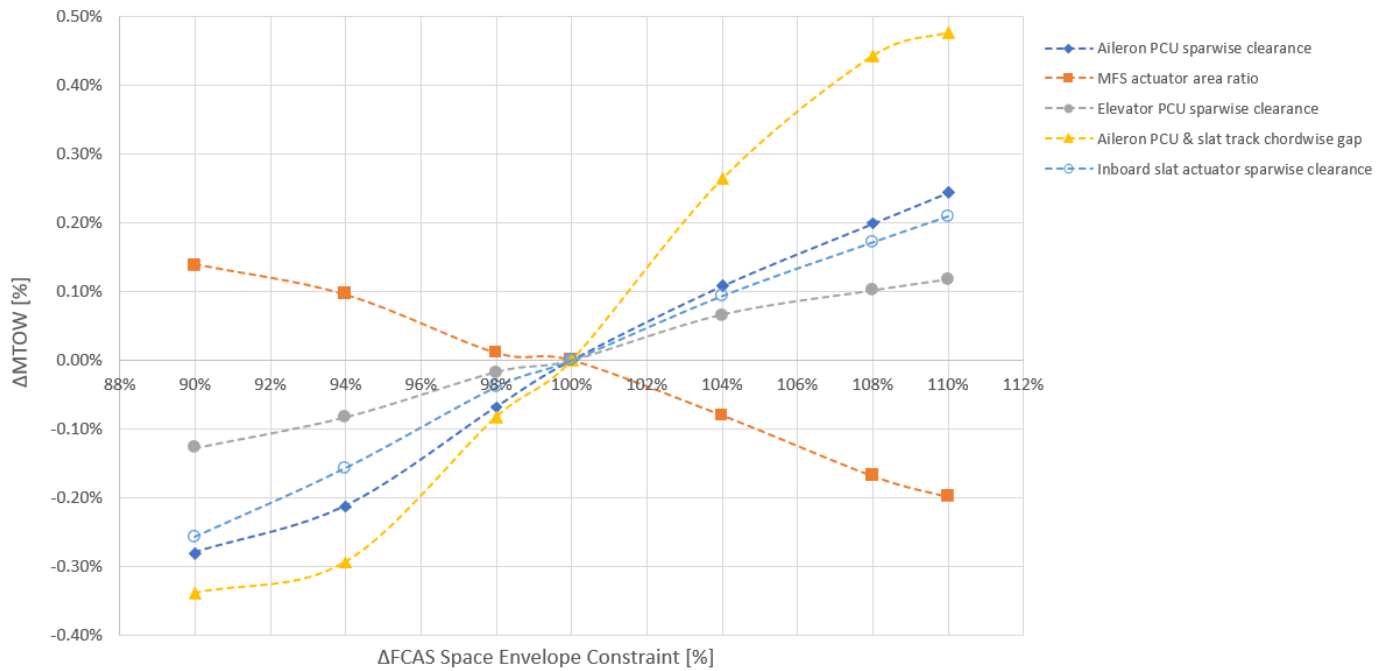


Figure 5.4: Sensitivity analysis results

From the results, it can be observed that:

- Aircraft weight is monotonically increasing with increasing FCASs constraints, except for MFS actuator area ratio. MTOW is most sensitive to the change of Aileron PCU & slat track chordwise gap constraint, partially due to its largest true value of change (2 inches for 10% of difference). MTOW is least sensitive to the change of Elevator PCU sparwise clearance, since this constraint only effects on horizontal tail instead of main wing.
- Outboard sparwise constraint has more significant impact than an inboard one, based on the observation that MTOW is more sensitive to aileron PCU sparwise clearance constraint than inboard slat actuator sparwise clearance constraint. This is expected since an increase in wingtip thickness implies an simultaneous increase in wing thickness to a greater extent.
- The Aileron PCU & slat track chordwise gap constraint is not active when its bound is at 90% of its reference value. This is likely caused by the discrepancy in decrease trend of MTOW.
- MTOW increases with decreasing MFS actuator area ratio, since the constraint forces the wing to expand in sparwise or chordwise direction. A discrepancy at 98% of reference constraint value is due to the true change in constraint value that's too small (0.8% for 2% of difference in area ratio).

Table 5.4: Sensitivity analysis results

		Δ MTOW
Aileron PCU sparwise clearance	+10%	+0.24%
	-10%	-0.28%
MFS actuator area ratio	+10%	-0.20%
	-10%	+0.14%
Elevator PCU sparwise clearance	+10%	+0.12%
	-10%	-0.13%
Aileron PCU & slat track chordwise gap	+10%	+0.48%
	-10%	-0.34%
Inboard slat actuator sparwise clearance	+10%	+0.21%
	-10%	-0.26%

5.3 Machine Learning-Based Sensitivity Analysis

This section explores the potential to generate MTOW response from CMDO workflow with varying constraint values rapidly, using a Machine Learning (ML) model. Although the CMDO optimization algorithm itself is surrogate-based, such investigation is still sought due to extra capabilities desired: To investigate MTOW sensitivity with isolated, continuous variance in constraint of interest over a desired range. The isolation here refers to holding other constraint values, instead of bounds as in Section 5.2, unchanged while varying the value of a constraint of interest.

A standalone ML model was developed using data from DoE points generated during CMDO executions. The training dataset used is a matrix formed by all constraint function evaluations from each CMDO loop, and the label is the corresponding objective function (MTOW) evaluation. To perform a prediction, a vector of constraint functions is fed into the trained model. To perform predictions with continuous variation in one constraint of

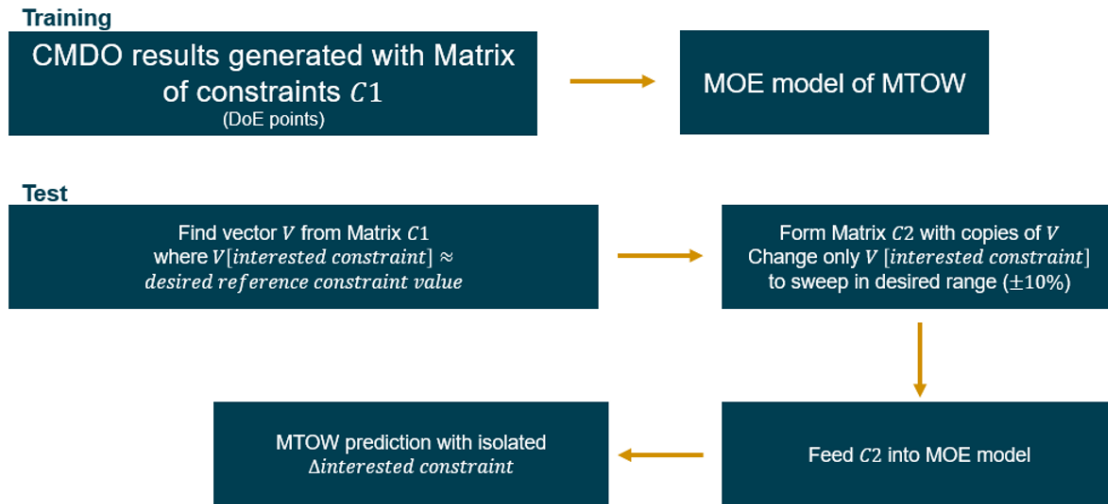


Figure 5.5: Training and prediction generation process for SEGOMOE ML model

interest, a matrix formed by the previous vector but with variation in the constraint of interest is input to the model. Figure 5.5 summarizes the training and prediction workflow.

A python implementation of the SEGOMOE algorithm is used to train the ML model and make predictions. As discussed in Section 4.2, the SEGOMOE-based ML model is constructed with the combination of local experts including Kriging, KPLS, polynomial regression, and radial basis functions.

In this study, 550 DoE points are used to train the model. Finally, the predicted MTOW sensitivity to two selected FCASs space envelope constraints are shown in Figure 5.6. Table 5.5 is created to compare results obtained from CMDO experiments and ML model prediction. It can be observed that the developed model generated correct data trends: MTOW increases with increasing aileron PCU clearance constraint and decreasing MFS actuator area ratio constraint. The model is also able to correctly predict that

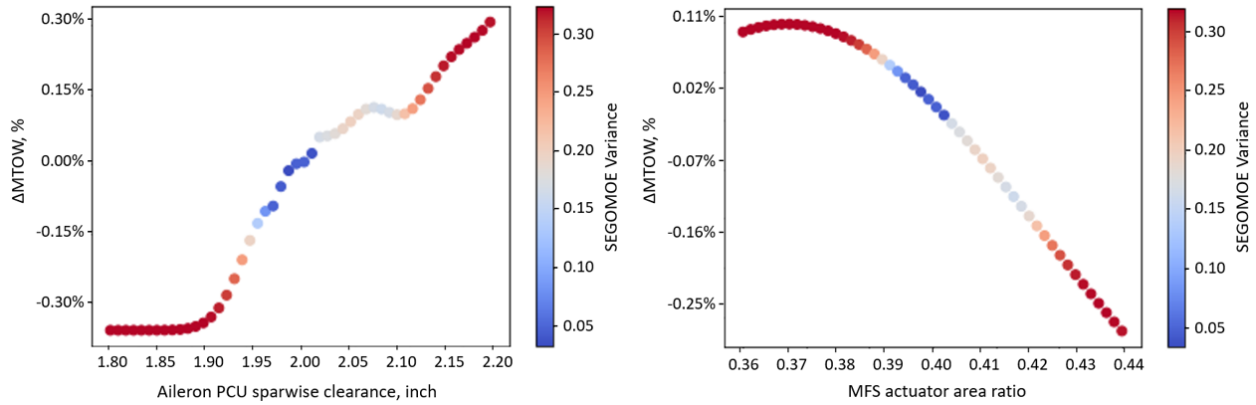


Figure 5.6: ML-based results for MTOW sensitivity to selected FCASs space envelope constraints

MTOW is more sensitive to aileron PCU sparwise clearance, comparing to MFS area ratio. One limitation of the model is the lack of quantitative accuracy: The deviation from experimental results ranges from 20% to 40%. However, the variance values given in Figure 5.6 shows the potential to further adapt the model using a larger training dataset size to improve prediction accuracy.

Table 5.5: MTOW sensitivity results comparison

		ΔMTOW response	
		Experiment	SEGOMOE
Aileron PCU sparwise	+10%	+0.24%	+0.30%
	-10%	-0.28%	-0.33%
MFS actuator area ratio	+10%	-0.20%	-0.28%
	-10%	+0.14%	+0.09%

Chapter 6

Summary and recommendations

In this work, a methodology to model and size the primary and secondary flight control actuation systems has been developed and integrated into an aircraft multidisciplinary design optimization environment for the conceptual design phase. A test case of business jet with aft mounted engines and T-tail design configuration was optimized with and without the developed FCASs sizing module. Comparison of the optimal designs demonstrated the impact of additional FCASs space envelope constraints on both design variables (aircraft design) and objective function (aircraft weight). Numerical experiments were conducted with different values of FCASs space envelope constraints to assess the sensitivity of object function; the most important constraint is the one linked to aileron PCU & slat track chordwise gap. A Machine Learning model was trained using MDO data. The predictions of the trained model demonstrated its capability to perform sensitivity

analysis on a qualitative basis much more rapidly.

The work has some limitations:

- A uniform sizing method is used for all PFC systems (aileron, elevator and rudder), which necessitates the use of different correction factors for different PFC systems, as introduced in Section 3.5. From the benchmark of PFC hinge moment estimation as shown in Figure 3.17, it can be seen that elevator and rudder end up with higher correction factor than aileron. This is due to the fact that these control surfaces have larger surface area and chord length, which leads to higher evaluation of equation 3.8 with similar M_{OM} which is an aircraft level parameter. The hinge moment evaluation for elevator is considered accurate after introduction of correction factor, since the variance found from benchmarking is low. On the other hand, with a high variance such evaluation for rudder is assumed inaccurate. The error propagates in the sizing procedure and the outcome is testified in Section 5.1: With the same lower bound requirements, the rudder actuator sparwise constraint is not active when similar constraints for aileron and elevator are active.
- The weight of the FACSs is currently not included in the weight prediction module within the CMDO environment. As a result, the change (increase) in MTOW summarized in Table 5.1 is conservative since it only take into account the change in wing thickness and planform design brought by FCASs implementation.

- The results of sensitivity analysis are influenced by the actual change of value of different constraints, when keeping a uniform percentage of change. The potential consequences are discussed in Section 5.2.
- The results generated from Machine Learning-based sensitivity analysis are based on MDO points, while the results generated from experiment-based sensitivity analysis were based on optimal designs. This difference contributes to the mismatch of results presented in Table 5.5.

The presence of winglets is not considered in this study, which is a common practice seen in many aircraft design problems at conceptual stage [6]. However, the addition of winglets consideration within the CMDO framework will improve the optimized design: Increased MTOW due to additional structural weight is expected, but the induced drag reduction will offset the negative weight effects and produce net benefits with respect to key performance metrics including maximum cruising range, maximum angle of attack and maximum rate of climb/descent [82].

Similar to many types of analysis methods and modules used in aircraft conceptual design, the developed FCASs space envelope prediction model is a low-fidelity tool. It has a fast calculation time but also inherent uncertainty. The found optimum might therefore be infeasible when re-evaluated using higher-fidelity analysis. Uncertainties in the FCASs sizing module need to be modelled to generate more reliable optima, thus performing uncertainty-based MDO.

In order to do this, the work in Section 3.5 provides an approach to model the FCASs sizing module uncertainties, and transforms the model output into random variables with CDF as exemplified in Figure 3.19. The FCASs space envelope constraint functions, generated from post-processing of FCASs sizing module output with deterministic output of other CMDO modules, are also uncertain functions. The high level description of the MDO problem can therefore be reformulated as a reliability-based one [83]:

$$\begin{aligned} & \min_{x \in \mathbb{R}^d} y(x) \\ \text{subject to} & \quad P(G_i(x) \leq 0) \geq \alpha_t \quad (i = 1, \dots, m) \\ & \quad c_j(x) \leq 0 \quad (j = 1, \dots, n) \end{aligned}$$

where $P(\bullet)$ is the probability measure, $G_i(x)$ are FCASs constraint functions, α_t is the target reliability, and $c_j(x)$ are deterministic constraints, respectively.

Bibliography

- [1] F. Grasso, *Multi-objective numerical optimization applied to aircraft design*. PhD thesis, Università degli Studi di Napoli Federico II, 2008.
- [2] K. Amadori, *On aircraft conceptual design: a framework for knowledge based engineering and design optimization*. PhD thesis, Institutionen för ekonomisk och industriell utveckling, Linköpings universitets, 2008.
- [3] J. Qiang, Y. Zhang, C. Haixin, and Y. Junke, “Aerodynamic optimization of a high-lift system with adaptive dropped hinge flap,” *Chinese Journal of Aeronautics*, vol. 35, no. 11, pp. 191–208, 2022.
- [4] P. K. Rudolph, “High-lift systems on commercial subsonic airliners,” Tech. Rep. NASA-CR-4746, National Aeronautics and Space Administration (NASA), 1996.
- [5] G. Nikas, “Fundamentals of sealing and tribology of hydraulic reciprocating seals,” *Proceedings of the IMechE*, 2008.

-
- [6] R. Priem, H. Gagnon, I. Chittick, S. Dufresne, Y. Diouane, and N. Bartoli, “An efficient application of Bayesian optimization to an industrial MDO framework for aircraft design,” in *AIAA Aviation 2020 Forum*, p. 3152, 2020.
- [7] J. M. Parr, A. J. Keane, A. I. Forrester, and C. M. Holden, “Infill sampling criteria for surrogate-based optimization with constraint handling,” *Engineering Optimization*, vol. 44, no. 10, pp. 1147–1166, 2012.
- [8] Dassault Systèmes Simulia Corp., *Isight 4.0 Component Guide*. Engineous software Inc., Cary, 2009.
- [9] R. T. Haftka, “Optimization of flexible wing structures subject to strength and induced drag constraints,” *AIAA Journal*, vol. 15, no. 8, pp. 1101–1106, 1977.
- [10] B. Grossman, R. Haftka, P.-J. Kao, D. Polen, M. Rais-Rohani, and J. Sobieszczanski-Sobieski, “Integrated aerodynamic-structural design of a transport wing,” *Journal of Aircraft*, vol. 27, no. 12, pp. 1050–1056, 1990.
- [11] S. Wakayama and I. Kroo, “Subsonic wing planform design using multidisciplinary optimization,” *Journal of Aircraft*, vol. 32, no. 4, pp. 746–753, 1995.
- [12] P. Rohl and D. Schrage, “Preliminary wing design of a high speed civil transport aircraft by multilevel decomposition techniques,” in *4th Symposium on Multidisciplinary Analysis and Optimization*, p. 4721, 1992.

-
- [13] E. J. Cramer, J. E. Dennis, Jr, P. D. Frank, R. M. Lewis, and G. R. Shubin, “Problem formulation for multidisciplinary optimization,” *SIAM Journal on Optimization*, vol. 4, no. 4, pp. 754–776, 1994.
- [14] J. R. Martins, J. J. Alonso, and J. J. Reuther, “A coupled-adjoint sensitivity analysis method for high-fidelity aero-structural design,” *Optimization and Engineering*, vol. 6, no. 1, pp. 33–62, 2005.
- [15] G. Kenway, G. Kennedy, and J. R. Martins, “A scalable parallel approach for high-fidelity aerostructural analysis and optimization,” in *53rd AIAA/ASME/ASCE/AHS/ASC Structures, Structural Dynamics and Materials Conference 20th AIAA/ASME/AHS Adaptive Structures Conference 14th AIAA*, p. 1922, 2012.
- [16] K. Leoviriyakit, S. Kim, and A. Jameson, “Aero-structural wing planform optimization using the Navier-Stokes equations,” in *10th AIAA/ISSMO Multidisciplinary Analysis and Optimization Conference*, p. 4479, 2004.
- [17] J. Martins and J. Alonso, “Aero-structural wing design optimization using high-fidelity sensitivity analysis,” *CEAS Conference on Multidisciplinary Aircraft Design Optimization*, 2001.

-
- [18] T. W. Simpson and J. R. Martins, “Multidisciplinary design optimization for complex engineered systems: report from a national science foundation workshop,” *Journal of Mechanical Design*, vol. 133, no. 10, 2011.
- [19] P. Piperni, A. DeBlois, and R. Henderson, “Development of a multilevel multidisciplinary-optimization capability for an industrial environment,” *AIAA journal*, vol. 51, no. 10, pp. 2335–2352, 2013.
- [20] H. Smith, D. Szirczák, G. Abbe, and P. Okonkwo, “The GENUS aircraft conceptual design environment,” *Proceedings of the Institution of Mechanical Engineers, Part G: Journal of Aerospace Engineering*, vol. 233, no. 8, pp. 2932–2947, 2019.
- [21] A. Seitz, *Advanced methods for propulsion system integration in aircraft conceptual design*. PhD thesis, Technische Universität München, 2012.
- [22] D. Bianchi, T. H. Orra, and P. Paglione, “Monte carlo based robust mdo applied to aircraft conceptual design: a technical-financial coupling optimization strategy,” in *15th AIAA Aviation Technology, Integration, and Operations Conference*, p. 2737, 2015.
- [23] D. Smith, A. Isikveren, R. Ajaj, and M. Friswell, “Multidisciplinary design optimization of an active nonplanar polymorphing wing,” in *27th Congress of the International Council of the Aeronautical Sciences*, vol. 1, pp. 529–539, 2010.

- [24] R. E. Perez, H. H. Liu, and K. Behdinan, “Multidisciplinary optimization framework for control-configuration integration in aircraft conceptual design,” *Journal of Aircraft*, vol. 43, no. 6, pp. 1937–1948, 2006.
- [25] J. Brezillon, A. Ronzheimer, D. Haar, M. Abu-Zurayk, M. Lummer, W. Kruger, and F. J. Natterer, “Development and application of multi-disciplinary optimization capabilities based on high-fidelity methods,” in *53rd AIAA/ASME/ASCE/AHS/ASC Structures, Structural Dynamics and Materials Conference 20th AIAA/ASME/AHS Adaptive Structures Conference 14th AIAA*, p. 1757, 2012.
- [26] N. Kroll, M. Abu-Zurayk, D. Dimitrov, T. Franz, T. Führer, T. Gerhold, S. Görtz, R. Heinrich, C. Ilic, J. Jepsen, *et al.*, “DLR project digital-x: towards virtual aircraft design and flight testing based on high-fidelity methods,” *CEAS Aeronautical Journal*, vol. 7, no. 1, pp. 3–27, 2016.
- [27] R. P. Henderson, J. R. Martins, and R. E. Perez, “Aircraft conceptual design for optimal environmental performance,” *The Aeronautical Journal*, vol. 116, no. 1175, pp. 1–22, 2012.
- [28] S. Choi, J. J. Alonso, I. M. Kroo, and M. Wintzer, “Multifidelity design optimization of low-boom supersonic jets,” *Journal of Aircraft*, vol. 45, no. 1, pp. 106–118, 2008.

- [29] M. Laban and U. Herrmann, “Multi-disciplinary analysis and optimisation applied to supersonic aircraft part 1: analysis tools,” in *48th AIAA/ASME/ASCE/AHS/ASC Structures, Structural Dynamics, and Materials Conference*, p. 1857, 2007.
- [30] S. Dean, J. Doherty, and T. Wallace, “MDO-based concept modelling and the impact of fuel systems on wing design,” in *47th AIAA Aerospace Sciences Meeting including the New Horizons Forum and Aerospace Exposition*, p. 434, 2009.
- [31] S. Guo, D. Li, and Y. Liu, “Multi-objective optimization of a composite wing subject to strength and aeroelastic constraints,” *Proceedings of the Institution of Mechanical Engineers, Part G: Journal of Aerospace Engineering*, vol. 226, no. 9, pp. 1095–1106, 2011.
- [32] E. Alyanak, R. Kolonay, P. Flick, N. Lindsley, and S. Burton, “Efficient supersonic air vehicle preliminary conceptual multi-disciplinary design optimization results,” in *12th AIAA Aviation Technology, Integration, and Operations (ATIO) Conference and 14th AIAA/ISSMO Multidisciplinary Analysis and Optimization Conference*, p. 5518, 2012.
- [33] A. Tfaily and M. Kokkolaras, “Integrating air systems in aircraft multidisciplinary design optimization,” in *2018 Multidisciplinary Analysis and Optimization Conference*, p. 3742, 2018.
- [34] C. Davies, M. Stelmack, P. S. Zink, A. De La Garza, and P. Flick, “High fidelity mdo process development and application to fighter strike conceptual design,” in *12th*

- AIAA Aviation Technology, Integration, and Operations (ATIO) Conference and 14th AIAA/ISSMO Multidisciplinary Analysis and Optimization Conference*, p. 5490, 2012.
- [35] B. Yan, P. Jansen, and R. Perez, “Multidisciplinary design optimization of airframe and trajectory considering cost, noise, and fuel burn,” in *12th AIAA Aviation Technology, Integration, and Operations (ATIO) Conference and 14th AIAA/ISSMO Multidisciplinary Analysis and Optimization Conference*, p. 5494, 2012.
- [36] R. Navaratne and J. Murugaiyan, “Multi-disciplinary optimization of flight trajectories,” in *2012 IEEE Aerospace Conference*, pp. 1–15, IEEE, 2012.
- [37] A. Ceruti, G. Caligiana, and F. Persiani, “Comparative evaluation of different optimization methodologies for the design of uavs having shape obtained by hot wire cutting techniques,” *International Journal on Interactive Design and Manufacturing (IJIDeM)*, vol. 7, no. 2, pp. 63–78, 2012.
- [38] L. Versiani Cabral, P. Paglione, and B. Silva de Mattos, “Multi-objective design optimization framework for conceptual design of families of aircraft,” in *44th AIAA Aerospace Sciences Meeting and Exhibit*, Aerospace Sciences Meetings, (Reno, NV, USA), January 2006.
- [39] N.-V. Nguyen, S.-M. Choi, W.-S. Kim, *et al.*, “Multidisciplinary unmanned combat air vehicle system design using multifidelity model,” *Aerospace Science and Technology*, vol. 26, no. 1, pp. 200–210, 2013.

- [40] B. Morrissey and R. McDonald, "Multidisciplinary design optimization of an extreme aspect ratio hale uav," in *9th AIAA Aviation Technology, Integration, and Operations Conference (ATIO)*, Aviation Technology, Integration, and Operations (ATIO) Conferences, (Hilton Head, SC, USA), September 2009.
- [41] D. Allison, C. Morris, J. Schetz, *et al.*, "A multidisciplinary design optimization framework for design studies of an efficient supersonic air vehicle," in *12th AIAA Aviation Technology, Integration, and Operations (ATIO) Conference and 14th AIAA/ISSMO Multidisciplinary Analysis and Optimization Conference*, Aviation Technology, Integration, and Operations (ATIO) Conferences, (Indianapolis, IN, USA), September 2012.
- [42] N. V. Nguyen, J.-W. Lee, M. Tyan, and D. Lee, "Possibility-based multidisciplinary optimisation for electric-powered unmanned aerial vehicle design," *The Aeronautical Journal*, vol. 119, no. 1221, pp. 1397–1414, 2015.
- [43] A. Mirzoyan, "Studies on MDO of engine design parameters with mission, noise and emission criteria at SSBJ engine conceptual design," in *26th International Congress of the Aeronautical Sciences, Anchorage, AK, USA*, 2008.
- [44] N. E. Antoine and I. M. Kroo, "Framework for aircraft conceptual design and environmental performance studies," *AIAA journal*, vol. 43, no. 10, pp. 2100–2109, 2005.

- [45] S. V. Subramanian and D. A. De Laurentis, “Application of multidisciplinary systems-of-systems optimization to an aircraft design problem,” *Systems Engineering*, vol. 19, no. 3, pp. 235–251, 2016.
- [46] U. Iemma and M. Diez, “Optimal conceptual design of aircraft including community noise prediction,” in *12th AIAA/CEAS Aeroacoustics Conference (27th AIAA Aeroacoustics Conference)*, p. 2621, 2006.
- [47] J. Longo, M. Sippel, G. Carrier, A. Loubeau, R. Jarlas, and D. Perigo, “Concept study for a mach 6 transport aircraft,” in *47th AIAA Aerospace Sciences Meeting including The New Horizons Forum and Aerospace Exposition*, p. 435, 2009.
- [48] K. Geiselhart, L. Ozoroski, J. Fenbert, E. Shields, and W. Li, “Integration of multifidelity multidisciplinary computer codes for design and analysis of supersonic aircraft,” in *49th AIAA Aerospace Sciences Meeting Including the New Horizons Forum and Aerospace Exposition*, p. 465, 2011.
- [49] Y. Deremaux, N. Pietremont, J. Negrier, E. Herbin, and M. Ravachol, “Environmental MDO and uncertainty hybrid approach applied to a supersonic business jet,” in *12th AIAA/ISSMO Multidisciplinary Analysis and Optimization Conference*, p. 5832, 2008.
- [50] E. Safavi, M. Chaitanya, J. Ölvander, and P. Krus, “Multidisciplinary optimization of aircraft actuation system for conceptual analysis,” in *51st AIAA Aerospace Sciences*

- Meeting including the New Horizons Forum and Aerospace Exposition*, Aerospace Sciences Meetings, (Grapevine (Dallas/Ft. Worth Region), TX, USA), January 2013.
- [51] C. Jouannet and P. Krus, “Direct simulation based optimization for aircraft design including systems,” in *11th AIAA/ISSMO Multidisciplinary Analysis and Optimization Conference*, Multidisciplinary Analysis Optimization Conferences, (Portsmouth, VA, USA), September 2006.
- [52] E. Safavi, M. Tarkian, H. Gavel, and J. Ölvander, “Collaborative multidisciplinary design optimization: a framework applied on aircraft conceptual system design,” *Concurrent Engineering*, vol. 23, no. 3, pp. 236–249, 2015.
- [53] R. Peoples and K. Willcox, “Value-based multidisciplinary optimization for commercial aircraft design and business risk assessment,” *Journal of Aircraft*, vol. 43, no. 4, pp. 913–921, 2006.
- [54] N. Davendraingam and W. Crossley, “Robust optimization of aircraft design and airline network design incorporating econometric trends,” in *11th AIAA Aviation Technology, Integration, and Operations (ATIO) Conference, including the AIAA Balloon Systems Conference and 19th AIAA Lighter-Than*, p. 6927, 2011.
- [55] S. Chai and W. Mason, “Landing gear integration in aircraft conceptual design,” in *6th Symposium on Multidisciplinary Analysis and Optimization*, p. 4038, 1996.

- [56] A. Tfaily, K. Huynh, P. Piperni, and S. Liscouet-Hanke, "Landing gear integration in an industrial multi-disciplinary optimization environment," *SAE Technical Paper*, no. 2013-01-2319, 2013.
- [57] A. Papageorgiou, M. Tarkian, K. Amadori, and J. Ölvander, "Multidisciplinary optimization of unmanned aircraft considering radar signature, sensors, and trajectory constraints," *Journal of Aircraft*, vol. 55, no. 4, pp. 1629–1640, 2018.
- [58] A. Papageorgiou, J. Ölvander, and K. Amadori, "Development of a multidisciplinary design optimization framework applied on UAV design by considering models for mission, surveillance, and stealth performance," in *18th AIAA/ISSMO Multidisciplinary Analysis and Optimization Conference*, p. 4151, 2017.
- [59] J. L. Felder, G. V. Brown, H. D. Kim, and J. Chu, "Turboelectric distributed propulsion in a hybrid wing body aircraft," in *Proceedings of the International Symposium on Air Breathing Engines Conference*, pp. 1–20, 2011.
- [60] A. Teo, K. Rajashekara, J. Hill, and B. Simmers, "Examination of aircraft electric wheel drive taxiing concept," in *Proceedings of the SAE Power Systems Conference*, pp. 1–5, 2008.
- [61] K. Munoz-Ramos *et al.*, "Electrical analysis of proton exchange membrane fuel cells for electrical power generation onboard commercial airplanes," in *Proceedings of the IEEE Transportation Electrification Conference and Expo*, pp. 1–6, 2012.

- [62] V. Viswanathan and B. M. Knapp, "Potential for electric aircraft," *Nature Sustainability*, vol. 2, pp. 88–89, Feb. 2019.
- [63] A. Diaz Puebla and R. C. Munjulury, "Sizing of actuators for flight control systems and flaps integration in RAPID," tech. rep., Linköping University, Department of Management and Engineering, Fluid and Mechatronic Systems, Linköping, Sweden, 2015.
- [64] R. C. Munjulury, I. E. Andrés, A. D. Puebla, and P. Krus, "Knowledge-based flight control system and control surfaces integration in RAPID," in *Aerospace Technology Congress*, vol. 2016, 2016.
- [65] S. Frischemeier, "Electrohydrostatic actuators for aircraft primary flight control-types, modelling and evaluation," in *5th Scandinavian International Conference on Fluid Power, Linköping, Sweden*, 1997.
- [66] S. Wu, B. Yu, Z. Jiao, Y. Shang, and P. Luk, "Preliminary design and multi-objective optimization of electro-hydrostatic actuator," *Proceedings of the Institution of Mechanical Engineers, Part G: Journal of Aerospace Engineering*, vol. 231, no. 7, pp. 1258–1268, 2017.
- [67] L. Xue, S. Wu, Y. Xu, and D. Ma, "A simulation-based multi-objective optimization design method for pump-driven electro-hydrostatic actuators," *Processes*, vol. 7, no. 5, p. 274, 2019.

-
- [68] J. Fu, J.-C. Maré, and Y. Fu, “Modelling and simulation of flight control electromechanical actuators with special focus on model architecting, multidisciplinary effects and power flows,” *Chinese Journal of Aeronautics*, vol. 30, no. 1, pp. 47–65, 2017.
- [69] G. Di Rito, E. Denti, and R. Galatolo, “Object-oriented modelling of flight control actuation systems for power absorption assessment,” in *Proceedings of the 27th Congress of the International Council of the Aeronautical Sciences (ICAS)*, vol. 7, p. 2, 2010.
- [70] I. Moir and A. Seabridge, *Design and development of aircraft systems*. John Wiley & Sons, 2012.
- [71] M. Prasad and K. Gangadharan, “Aileron endurance test rig design based on high fidelity mathematical modeling,” *CEAS Aeronautical Journal*, vol. 8, no. 4, pp. 653–671, 2017.
- [72] A. Van der Velden and P. Koch, “Isight design optimization methodologies,” *ASM Handbook*, vol. 22, p. 79, 2010.
- [73] J. Roskam, *Airplane design*. DAR corporation, 1985.
- [74] M. H. Sadraey, *Aircraft design: A systems engineering approach*. John Wiley & Sons, 2012.
- [75] A. K. Kundu, *Aircraft design*. Cambridge University Press, 2010.
- [76] J. Russell, *Performance and stability of aircraft*. Butterworth-Heinemann, 1996.

-
- [77] A. I. Forrester and A. J. Keane, “Recent advances in surrogate-based optimization,” *Progress in aerospace sciences*, vol. 45, no. 1-3, pp. 50–79, 2009.
- [78] A. G. Watson and R. J. Barnes, “Infill sampling criteria to locate extremes,” *Mathematical Geology*, vol. 27, no. 5, pp. 589–608, 1995.
- [79] D. R. Jones, M. Schonlau, and W. J. Welch, “Efficient global optimization of expensive black-box functions,” *Journal of Global Optimization*, vol. 13, no. 4, pp. 455–492, 1998.
- [80] M. J. Sasena, P. Papalambros, and P. Goovaerts, “Exploration of metamodeling sampling criteria for constrained global optimization,” *Engineering Optimization*, vol. 34, no. 3, pp. 263–278, 2002.
- [81] N. Bartoli, T. Lefebvre, S. Dubreuil, R. Olivanti, R. Priem, N. Bons, J. R. Martins, and J. Morlier, “Adaptive modeling strategy for constrained global optimization with application to aerodynamic wing design,” *Aerospace Science and Technology*, vol. 90, pp. 85–102, 2019.
- [82] F. Afonso, J. Vale, F. Lau, and A. Suleman, “Performance based multidisciplinary design optimization of morphing aircraft,” *Aerospace Science and Technology*, vol. 67, pp. 1–12, 2017.

- [83] H.-U. Park, J.-W. Lee, J. Chung, and K. Behdinan, “Uncertainty-based MDO for aircraft conceptual design,” *Aircraft Engineering and Aerospace Technology: An International Journal*, vol. 87, no. 4, pp. 345–356, 2015.